Journal of Colloid And Interface Science

Multifunctional interfaces for multiple uses: tin(II)-hydroxyapatite for reductive adsorption of Cr(VI) and its upcycling into catalyst for air protection reactions

--Manuscript Draft--

Manuscript Number:	JCIS-22-6058
Article Type:	Full length article
Section/Category:	C. Adsorption, Catalysis and Electrochemistry
Keywords:	Cr(VI) removal, wastewaters; ecofriendly materials; reuse; circular economy; environmental catalysis
Corresponding Author:	Sebastiano Campisi, Ph.D. University of Milan Milano, ITALY
First Author:	Sebastiano Campisi, Ph.D.
Order of Authors:	Sebastiano Campisi, Ph.D.
	Mirko Leone
	Maddalena Papacchini
	Claudio Evangelisti
	Laura Polito
	Georgeta Postole
	Antonella Gervasini
Abstract:	Evidence collected to date has demonstrated that tin(II)-functionalized hydroxyapatites (Sn/HAP) are a newly discovered class of ecofriendly reductive adsorbents for Cr(VI) removal from wastewaters. In this work an upgraded series of Sn/HAP materials assured a maximum removal capacity of ≈ 20 mg Cr /g, doubling the previously reported value for Sn/HAP materials, thanks to higher Sn-dispersion as proved by X-ray photoelectron spectroscopy and electron microscopy. Insights on kinetics and thermodynamics of the reductive adsorption process are provided and the influence of pH, dosage, and nature of Cr(V) precursors on chromium removal performances have been investigated. Pseudo-second-order kinetics described the interfacial reductive adsorption process on Sn/HAP, characterized by low activation energy (21 kJ mol -1), when measured in the 278 – 318 K interval. Sn/HAP did not necessitate highly acidic environment to operate the reductive adsorption reaction; tests performed in the 2 - 6 pH interval showed similar efficiency in terms of Cr(VI) removal. Conventional procedures of recycling and regeneration resulted ineffective in restoring the pristine performances of the samples due to surface presence of both Sn(IV) and Cr(III). To overcome these weaknesses, the used samples (Sn+Cr/HAP) were upcycled into catalysts in a circular economy perspective. Used samples were tested as catalysts in gas-phase environmental reactions: selective catalytic reduction of NO x (NH 3 -SCR), NH 3 selective catalytic Oxidation (NH 3 -SCO), and selective catalytic oxidation of methane to CO 2 . Catalytic tests enlightened the interesting activity of the upcycled Sn+Cr/HAP samples in catalytic oxidation processes, being able to selectively oxidize methane to CO 2 at relatively low temperature.
Suggested Reviewers:	Guylène Costentin, Ph.D. Sorbonne University Pierre and Marie Curie Campus guylene.costentin@upmc.fr Expert in hydroxyapatite-based materials
	Michele Ferri, Ph.D. Italian Institute of Technology Michele.Ferri@iit.it

	Expert in hydroxyapatite-based materials and adsorption processes for wastewater remediation
	Pierangela Cristiani, Ph.D. Ricerca Sul Sistema Energetico RSE SPA Pierangela.Cristiani@rse-web.it Expert in biomaterials and processes for water remediation
	Simone Sprio, Ph.D. Institute of Science and Technology of Ceramic Materials National Research Council simone.sprio@istec.cnr.it Expert in hydroxyapatite-based materials
	Jean-François Lamonier, Professor Université Lille1 Sciences and Technologies Library jean-francois.lamonier@univ-lille.fr Expert in hydroxyapate-based catalysts for air protection reactions

UNIVERSITÀ DEGLI STUDI DI MILANO
DIPARTIMENTO DI CHIMICA

Milano, 5th August 2022

To *Journal of Colloid and Interface Science* Journal
Prof. Martin Malmsten
University of Copenhagen Department of Pharmacy,
København, Denmark
Editor-in-Chief of *Journal of Colloid and Interface Science*, Elsevier

Dear Prof. Malmsten,

We wish to submit our manuscript entitled "*Multifunctional interfaces for multiple uses: tin(II)-hydroxyapatite for reductive adsorption of Cr(VI) and its upcycling into catalyst for air protection reactions*" to be considered for publication as research article in the ***Journal of Colloid and Interface Science***.
In this study we optimized the Cr(VI) removal capacity of tin(II)-modified hydroxyapatite (Sn/HAP), an interesting material recently studied by our research group in the reductive adsorption of Cr(VI). In this study particular attention has been devoted to optimizing not only the Cr(VI) removal performance but also the entire adsorbent value chain, from the synthesis to the after-life of the used sorbents. Hydroxyapatite, a stable and low-cost biomaterial, was synthesized by cheap precursors and then functionalized by tin(II) deposition from aqueous solutions. The obtained materials were characterized by higher surface area which assured an enhanced tin(II) phase dispersion. This allowed to double the Cr(VI) removal capacity (20 mg g^{-1}) compared to Sn/HAP materials previously presented in the literature (10 mg g^{-1}). In addition, the used Sn+Cr/HAP materials have been recovered and re-used in a second step as catalysts in reactions of environmental protection (e.g. denitrification of gaseous emissions, de-NOx, and oxidation of organic compounds). These promising results could open the way to a "circular economy" perspective in the environmental remediation field.
We believe then that this study fits well to several categories of ***Journal of Colloid and Interface Science*** and could be of interest to the readers of your journal and in general to all the scientists, who work in the fields of adsorption and catalysis.
The research work was in part supported by a grant from INAIL ((Istituto Nazionale Assicurazione Infortuni sul Lavoro, Italy).
We confirm that this manuscript is original, has not been published elsewhere and is not under consideration by another journal.
All authors have approved the manuscript and agree with its submission to *Journal of Colloid and Interface Science*. The authors have no conflicts of interest to declare.
Please address all correspondence concerning this manuscript to Prof. Antonella Gervasini (antonella.gervasini@unimi.it) and Dr. Sebastiano Campisi (sebastiano.campisi@unimi.it).
We hope that our manuscript can have a positive impact on Editors and Reviewers and we are waiting for your decision on the suitability of the manuscript for publication in *Journal of Colloid and Interface Science*.

Dipartimento di Chimica
Via Golgi, 19 - 20133 Milano, Italy
indirizzomail@unimi.it

UNIVERSITÀ DEGLI STUDI DI MILANO
DIPARTIMENTO DI CHIMICA

With sincerely best regards,

Prof. Antonella Gervasini (ORCID: 0000-0001-6525-7948)

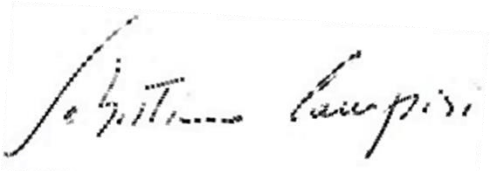

Dr. Sebastiano Campisi (ORCID: 0000-0002-5496-7482)

Dipartimento di Chimica
Via Golgi, 19 - 20133 Milano, Italy
indirizzomail@unimi.it

3: Graphical Abstract

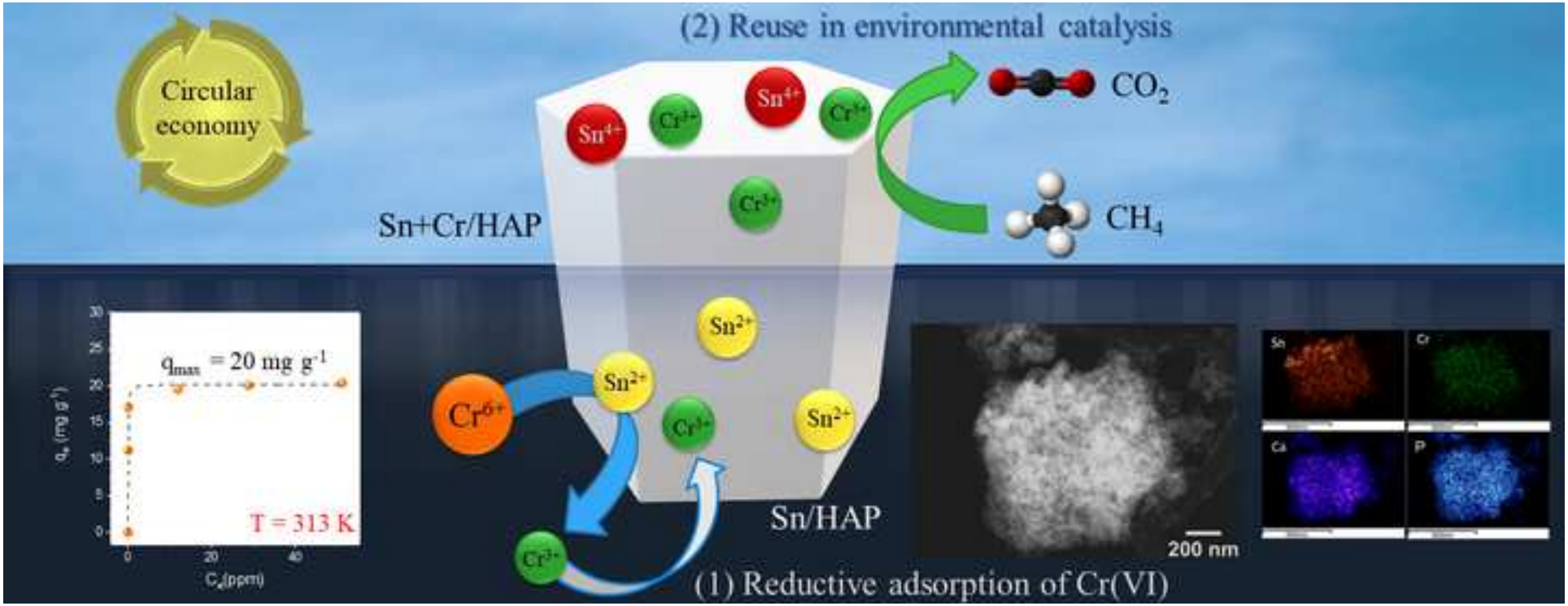

Multifunctional interfaces for multiple uses: tin(II)-hydroxyapatite for reductive adsorption of Cr(VI) and its upcycling into catalyst for air protection reactions

Sebastiano Campisi,[a,*] Mirko Leone,[a] Maddalena Papacchini,[b] Claudio Evangelisti,[c] Laura Polito,[d] Georgeta Postole[e] and Antonella Gervasini[a,*]

[a] Dipartimento di Chimica, Università degli Studi di Milano, Via Golgi 19, 20133 Milano, Italy

[b] Department of Technological Innovations and Safety of Plants, INAIL, Products and Anthropic Settlements, Via di Fontana Candida 1, Monte Porzio Catone, 00078 Rome, Italy

[c] CNR - ICCOM - Istituto di Chimica dei Composti OrganoMetallici, Via G. Moruzzi 1, I-56124 Pisa, Italy

[d] CNR - Consiglio Nazionale delle Ricerche, SCITEC - Istituto di Scienze e Tecnologie Chimiche "Giulio Natta", Via G. Fantoli 16/15, 20138 Milano, Italy

[e] Univ Lyon, Université Claude Bernard Lyon 1, CNRS, IRCELYON, F-69626, Villeurbanne, France

* *Corresponding authors*

sebastiano.campisi@unimi.it

antonella.gervasini@unimi.it

Graphical abstract

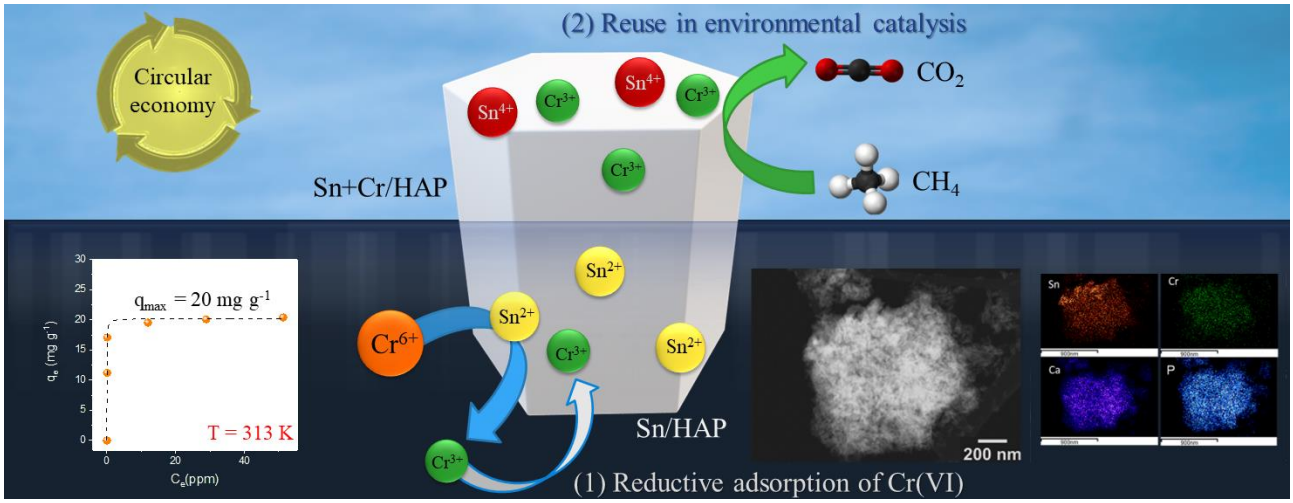

Abstract

Evidence collected to date has demonstrated that tin(II)-functionalized hydroxyapatites (Sn/HAP) are a newly discovered class of ecofriendly reductive adsorbents for Cr(VI) removal from wastewaters.

In this work an upgraded series of Sn/HAP materials assured a maximum removal capacity of ≈ 20 mg_{Cr}/g, doubling the previously reported value for Sn/HAP materials, thanks to higher Sn-dispersion as proved by X-ray photoelectron spectroscopy and electron microscopy.

Insights on kinetics and thermodynamics of the reductive adsorption process are provided and the influence of pH, dosage, and nature of Cr(V) precursors on chromium removal performances have been investigated. Pseudo-second-order kinetics described the interfacial reductive adsorption process on Sn/HAP, characterized by low activation energy (21 kJ mol^{-1}), when measured in the 278 – 318 K interval.

Sn/HAP did not necessitate highly acidic environment to operate the reductive adsorption reaction; tests performed in the 2 - 6 pH interval showed similar efficiency in terms of Cr(VI) removal.

Conventional procedures of recycling and regeneration resulted ineffective in restoring the pristine performances of the samples due to surface presence of both Sn(IV) and Cr(III). To overcome these weaknesses, the used samples (Sn+Cr/HAP) were upcycled into catalysts in a *circular economy* perspective.

Used samples were tested as catalysts in gas-phase environmental reactions: selective catalytic reduction of NO_x (NH_3-SCR), NH_3 selective catalytic Oxidation (NH_3-SCO), and selective catalytic oxidation of methane to CO_2. Catalytic tests enlightened the interesting activity of the upcycled Sn+Cr/HAP samples in catalytic oxidation processes, being able to selectively oxidize methane to CO_2 at relatively low temperature.

KEYWORDS: Cr(VI) removal, wastewaters; ecofriendly materials; reuse; circular economy; environmental catalysis

1. Introduction

Among heavy metal pollutants in groundwaters and soils chromium is considered as one of the most harmful substances. Although Cr can be found in different oxidation states ranging from +2 to +6, it is prevalently detected in the environment in the most stable two forms Cr(III) and Cr(VI). Due to the greater solubility in water, stronger migration and higher oxidative capacity compared to trivalent chromium and the deriving carcinogen, teratogen and mutagen properties, exposure to high concentration of hexavalent chromium (Cr(VI)) poses serious threats to the ecosystem and human health [1]. Cr(VI) species (such as dichromate, chromate, chromic acid, and hydrogen chromate) are released from both natural and anthropogenic sources, such as industrial activities connected with metal plating, cooling-tower, water additives, leather tanning, industrial coolants [2]. Since it is not possible to exert any control on natural emissions, regulating industrial emissions and keeping hexavalent chromium species at lowest exposure levels become a high priority to minimize the related environmental and health risks. In Europe, the admissible concentration values of Cr (VI) are regulated on a national scale and range from 0.05 to 2 mg L^{-1} [3]. Therefore, intensive research efforts have been devoted and are indeed ongoing, to develop technologies able to comply with such discharge limits.

Reductive adsorption is one of the first-line treatment strategies for the hexavalent chromium (Cr(VI)) pollution remediation [4]. Being the combination of Cr(VI) reduction reaction and adsorption, this approach synergically joins the advantages of the two separate processes (i.e. chemical reduction and adsorption). Indeed, under the best circumstances, reductive adsorption generates an ion-free and decontaminated water and a spent solid adsorbent. The latter retains chromium in the form of less toxic Cr(III) species which assures a safer and easier disposal. The ideal material to be used as sorbent in reductive adsorption should possess a multifunctional interface, where both centers with reducing activity

towards Cr(VI) and anchoring sites for Cr(III) species are exposed. Despite single materials having a significant reductive ability have been proposed, in most cases these materials are hampered by a limited adsorption capacity (fast saturation), poor selectivity for Cr(VI)/Cr(III) (Guan et al., 2015), tendency to undergo partial dissolution, passivation or agglomeration in aqueous solution. Thus, to date the list of suitable candidates as reductive adsorbents encompasses prevalently hybrid materials. In the latter, the reducing phase is dispersed onto high-surface area materials, that can act as adsorbents. Typically, hybrid materials include one or more of the following components: i) organic amendments (e.g. gallic acid, humic acid, tartaric acid, caffeic acid) [5–8] and polymers (e.g. polyaniline)[5,9–14], ii) sulfur-based materials (e.g. FeS, H_2S, etc.)[15–17], iii) iron-containing phases (iron oxides, nano zero-valent iron nanoparticles nZVI)[6,9,11,12,17–30], iv) inorganic nanoparticles (zero-valent Al NPs, Pd NPs, CuFe and NiFe alloyed NPs)[31–35]. Recently, there is much impetus to develop ecofriendly adsorbents [36], such as biochar [19,21,22,24,26,27,29,30,37–39] and other waste-derived materials [40–43]. Within this trend fits hydroxyapatite ($Ca_{10}(PO_4)_6(OH)_2$, HAP), an inorganic and sustainable material that can derive from biowastes or be synthesized from low-cost precursors. The applications of HAP in environmental catalysis and water remediation have increased significantly in the last few years [44]. As its surface holds numerous functional groups (hydroxyl, phosphate and carbonate groups), the application of hydroxyapatite in adsorption processes for heavy metal removal from wastewaters can be considered a valuable approach. Actually, heavy metals including Pb(II), Cu(II), Cd(II), Cr(III), were successfully sequestered by HAP according to several sorption mechanisms, the dominant ones being surface complexation, dissolution-precipitation and ion exchange [45–49]. Unfortunately these mechanisms are scarcely active in immobilizing Cr(VI) species onto HAP. To improve Cr(VI) removal efficiency, the combination of hydroxyapatite with other materials, such as cellulose, chitin, alginate, graphene oxide and iron phases has been proposed [18,50–55].

A recent work has demonstrated that tin(II)-functionalized hydroxyapatites (Sn/HAP) are a newly discovered class of ecofriendly reductive adsorbents effective in reducing Cr(VI) and adsorbing Cr(III) according to a pure heterogenous interfacial process. Cr(VI) removal up to 10 mg/g was attained on Sn/HAP with 15 wt% Sn(II) through a dual mechanism, involving the reduction of Cr(VI) by Sn(II) phase and the subsequent immobilization of the formed Cr(III) species, as proved by electron microscopy and XPS analyses [49]. Unfortunately, once all exposed Sn(II) centers have been converted to Sn(IV) and all the surface sites are occupied by Cr(III) species, the adsorbent is inactive and should be regenerated. However, a regeneration treatment able to restore the pristine Sn(II) oxidation state and at the same time to make accessible new adsorption sites for Cr(III) would be too expensive and challenging to be implemented.

In this work efforts were devoted to enhance the Cr(VI) removal capacity and to overcome the lack of regenerability currently limiting the Sn/HAP materials. To develop Sn/HAP materials with enhanced Cr(VI) removal capacity, tin(II) phase was deposited onto synthetic hydroxyapatite with relatively high surface area to improve tin dispersion. In addition, an alternative strategy, consisting in upcycling the used adsorbents into catalysts for gas-phase environmental reactions is proposed to overpass the limitation of difficult regeneration and, most importantly, to implement a circular economy approach in the environmental remediation field.

2. Materials and Methods

2.1 Materials

Calcium nitrate tetrahydrate ($Ca(NO_3)_2 \cdot 4H_2O$, 98%), ammonia solution 30%, stannous chloride dihydrate ($SnCl_2 \cdot 2H_2O$, 98%), potassium bichromate ($K_2Cr_2O_7$, 99%), sodium bichromate ($Na_2Cr_2O_7$, 99%) were all purchased from Carlo Erba. Diammonium hydrogen phosphate ($(NH_4)_2HPO_4$, 99.2 %) was from VWR. 1,5-diphenylcarbazide (DPC, ACS reagent), acetone (for analysis, ExpertQ®, ACS, ISO, Reag. Ph. Eur.), and hydrochloric acid 37% were from Merck. All reagents are of analytical grade and used without further purification. All the aqueous solutions were prepared in MilliQ water.

Gaseous species as nitrogen (N_2, 99.9995%), air (grade R), H_2 (grade R), 1,00% mol/mol ammonia in nitrogen, 2.04% mol/mol nitrogen monoxide in nitrogen, 5% CH_4 in He, were supplied by Sapio.

2.2 Preparation of Sn/HAP

Bare hydroxyapatite (HAP) samples were synthesized by conventional precipitation method as reported in the literature [48] and detailed in SI (Par. S.1.1).

Tin-hydroxyapatites with Sn nominal loading in the range between 25 and 150 mg Sn/g (0.2 – 1.3 mmol Sn/g) were prepared from a tin-containing aqueous solution by using a validated *flash* deposition technique already used successfully for iron deposition on HAP [49,56,57] and described in SI (Par. S.1.2). The code SnX/HAP was used for sample labelling, where X represents the nominal Sn content (expressed as wt.%). Acid digestion of solid samples was performed using 3 mL HCl 37 wt%. at 120°C and concentrating the solution to ca. 1 mL, then diluting 1:1000 with MilliQ water.

2.3 Material characterization

The determination of Sn and Cr content in solid samples was performed through the Inductively Coupled Argon Plasma – Optical Emission Spectroscopy (ICP-OES) on the

153 solutions obtained from solid digestion, using an ICP - Optical Emission dual view
154 Spectrophotometer (Perkin - Elmer, Model Optima 8000 DS), equipped with an
155 autosampler and using argon as internal standard.

156 Morphological and structural analyses were performed through transmission electron
157 microscopy (TEM). ZEISS LIBRA 200FE microscope with a 200 kV FEG source, in column
158 second-generation omega filter was used for TEM. EDX spectra and element maps were
159 collected along with HAADF-STEM micrographs.

160 N_2 (99.9995 % purity from SAPIO) adsorption-desorption isotherms were collected at the
161 liquid nitrogen temperature on a Sorptomatic 1990 (by Thermo Scientific) to measure
162 surface area and porosity by using samples with controlled grain size (74-177 μm).

163 X-Ray powder diffraction (XRPD) patterns were collected using a PANanalytical XPert
164 PRO powder diffractometer operating with an X-ray source at 40 kV and 25 mA in the range
165 between 5 °- 65 °(2θ), step of 0.033 °2θ and collection time of 50 s.

166 XPS spectra were acquired by a KRATOS AXIS ULTRA DLD spectrometer (Kratos
167 Analytical) equipped with a magnetic immersion lens, a hemispherical analyzer and a delay
168 line detector. The procedure for the interpretation of the C 1s peaks and quantitative
169 determination of the surface species did not take into account the bands of adventitious
170 carbon (284.8 eV) and only the bands due to carbonate groups (ca. 289 eV) were considered.

171 Further details on the characterization analyses and sample preparation procedures are
172 available in the Supplementary materials (Par. S.1.3).

173 *2.4 Batch Cr(VI) removal experiments*

174 SnX/HAP samples with different nominal tin content (2.5, 5, 7.5, 10, 12.5, 15 wt.%) were
175 tested in batch experiments for Cr(VI) removal under typical conditions of dosage (4.5 g/L),
176 pH value (pH = 2), initial Cr(VI) concentration (50 mg/L), and temperature (313 K) under
177 magnetic stirrer in air flux. Then, some parameters were varied as: initial Cr(VI)
178 concentration (80, 100, 150 mg/L; with fixed dosage, 4.5 g L^{-1}; pH value, 2; temperature,

313 K,; and contact time, 4h), pH values (2.0, 9.0 and natural – ca. 6.0; with fixed initial Cr(VI) concentration, 100 ppm; dosage, 4.5 g L^{-1}; temperature, 313 K; contact time, 4h), dosage (0.5, 1.0, 4.5 and 9 g L^{-1}; with fixed Cr(VI) concentration, 100 ppm; pH value, 2; temperature, 313 K; and contact tome, 4h), and temperature (278–318 K).

Adsorption isotherm on Sn12.5/HAP sample (dosage 4.5 g L^{-1}) was collected at 313 ± 0.1 K and pH value of 2 varying Cr(VI) initial concentrations in a 20-150 ppm range.

2.5 Analytical methods

The performances of the tested materials towards Cr(VI) removal were evaluated in terms of percent efficiency (%) and removal capacity (q, $mg_{Cr} \cdot g^{-1}$), calculated as reported in equations 1 and 2:

$$\text{Percent removal efficiency (\%)} = \frac{[Cr(VI)]^\circ - [Cr(VI)]_f}{[Cr(VI)]^\circ} \cdot 100 \qquad (1)$$

$$q\ (mg_{Cr}/g) = \frac{[Cr(VI)]^\circ - [Cr(VI)]_f}{m_{ads}} \cdot V_{sol} \qquad (2)$$

where $[Cr(VI)]^\circ$ and $[Cr(VI)]_f$ are the Cr(VI) initial and final concentration, respectively, expressed in ppm (mg/L), m_{ads} is the adsorbent mass, expressed in grams, and V_{sol} is the volume of the Cr(VI) solution, expressed in liters.

The determination of Cr(VI) concentration was performed by spectrophotometric analysis upon the reaction of the chromium-containing solution with the chromogenic species 1,5-diphenylcarbazide (DPC), according to the standard method BS EN 196-10:2006 [58]. Determinations of total Cr content in solution and on the used solids, after acid digestion, was determined by ICP-OES.

All the investigations were replicated to confirm reproducibility of the experimental results. In all cases the relative standard deviation values are of the order of ± 5%.

200 *2.6 Kinetic tests*

201 The kinetics of Cr(VI) reductive adsorption was studied by multiple batch tests of Cr(VI)
202 reduction-immobilization in different test tubes, by this way each point of the collected
203 kinetic profile as a function of time was obtained by independent tests. For a single batch
204 test, ca. 100 mg of freshly prepared Sn7.5/HAP was introduced in a plastic test tube with a
205 magnetic stir bar, whereas 22 mL of acidic potassium bichromate solution (pH 2, Cr(VI)
206 concentration of 100 ppm) were introduced in another test tube and both thermostated at
207 313 K. Once the solutions have been thermostated, the bichromate solution was added to the
208 test tube containing the Sn/HAP, and the reaction proceeded for a controlled time (from xx
209 to xx min) at 313 ± 0.1 K under air flux, after which the suspension was rapidly filtered and
210 the supernatant recovered to determine Cr(VI) concentration. The effect of temperature on
211 the kinetics of Cr(VI) reduction-adsorption was investigated in the 278–318 K range by
212 working at isoconversion, that is varying the time of each experiment at each temperature .

213 *2.7 Regeneration studies*

214 Regeneration procedures were carried out to control the reusability of the Cr(III)-Sn(IV)
215 containing Sn/HAP samples after use. Two different processes were investigated: reductive
216 treatment by hydroxylamine in liquid phase and reductive treatment by hydrogen in gas
217 phase.

218 In the first approach, about 18 mg of $HONH_2 \cdot HCl$ (calculated considering ca. 20% molar
219 excess with respect to expected Sn(IV) content) were dissolved in 100 mL of MilliQ water,
220 and the solution acidified with HCl up to pH 2. The prepared solution was put in contact
221 with ca. 100 mg of used Sn/HAP at 313 K for 1 h. The solid sample was then recovered by
222 filtration, washed with 50 mL of degassed MilliQ water and dried under vacuum.

223 In the second approach, ca. 100 mg of used Sn/HAP was introduced in a hydrogenator at
224 room temperature and alternating cycles of vacuum and hydrogen at 1 bar were applied: 1.30
225 min vacuum, 1.30 min H_2, 1 min vacuum, 1 min H_2, 30 s vacuum and 30 s H_2.

226 *2.8 Catalytic tests*

227 Catalytic behavior of upcycled selected sample was evaluated in three different reactions,
228 namely NH_3-SCR, NH_3-SCO and methane oxidation. Catalytic tests were carried out in a
229 continuous reaction line equipped with a set of mass flow controllers, a tubular vertical
230 electric oven, a quartz tubular microreactor and an online FT-IR spectrophotometer with
231 multiple reflection gas cell (2.4 m path length) and DTGS detector for qualitative and
232 quantitative determination of the composition of fed and vented gaseous mixtures.

233 Prior to the catalytic tests, the recovered and used sample was calcined in air at 773 K for 1h
234 (heating ramp 1 K/min). A given mass of calcined sample (ca. 0.150 g) was pressed, crushed,
235 and sieved to obtain particles in the range 45–60 mesh (0.35–0.25 mm), and dried at 393 K
236 overnight. Then, catalyst pretreatment was performed in situ under O_2/N_2 flow (20.08%
237 v/v) at 3 NL h^{-1} at 393 K for 30 min. The catalytic activity was studied as a function of
238 temperature in the 393–773 K interval for both NH_3-SCR and NH_3-SCO, keeping constant
239 the concentration of fed gas mixture flowing at 6 NL·h^{-1} (GHSV of ca. 40.000 h^{-1}). In the
240 case of CH_4 oxidation, the catalytic activity was evaluated in the 573–1033 K temperature
241 window working at GHSV of ca. 60.000 h^{-1}. At each temperature, the effluent composition
242 was monitored for 60 min to assure the attainment of the steady-state reaction condition.
243 The temperature was increased at step in aleatory way using a ramp of 10 ◦C·min^{-1}. The fed
244 gas mixtures were prepared by mixing 500 ppm of NH_3, 500 ppm of NO and 10,000 ppm of
245 O_2 for NH_3-SCR tests; 500 ppm of NH_3 and 10,000 ppm of O_2 for NH_3-SCO tests; ca. 1500
246 ppm of CH_4 and 30000 ppm of O_2 for CH_4 oxidation tests. In all cases, nitrogen was used as
247 carrier gas. The total absorbance of all the IR active gaseous species (Gram–Schmidt) vented
248 by the reactor was continuously recorded as a function of time while reaction temperature
249 was changing. The concentrations of NH_3, NO, N_2O, NO_2, CH_4, CO_2 and CO were determined
250 considering the height of the peak of the absorbance lines selected for each species and
251 applying calibration factors. Further details can be found in Supplementary Material (S.1.).

3. Results and discussion

3.1 Tin(II)-hydroxyapatite materials

Tin(II)-functionalized hydroxyapatite samples with varied tin loading (SnX/HAP, with 2.5 < X /wt.% < 15) were prepared by *flash* wet deposition of tin(II) chloride on HAP at different Sn concentration (2 – 15 mM). Table 1 gathers the experimental Sn loading values as determined by ICP-OES. The experimental values are in all cases higher than the nominal ones (as determined by considering the weighed amount of $SnCl_2 \cdot H_2O$ and the mass of HAP powder used). This discrepancy can be ascribed to a partial HAP dissolution and consequent mass loss under the acidic conditions adopted during the Sn-deposition procedure (pH = 2). Indeed, it is known that HAP can undergo amorphization and/or dissolution in extremely acidic media (pH < 3) for a long time of contact [47].

Surface composition was explored by X-ray photoelectron spectroscopy (XPS). Fig. 1a reports an exemplificative XPS survey spectrum obtained for Sn15/HAP sample. The spectrum displays the typical photopeaks associated with O1s (532 eV), Sn 3d (490 eV), Ca 2p (350 eV), P 2p (133 eV) and C1s (288.5 eV), the latter deriving from carbonate incorporation onto HAP surface. The tin surface concentration gradually increases as the bulk Sn concentration rises (Table 1). However, it is noteworthy that HAP surface seems approaching tin saturation around a maximum value of Sn bulk content of ca. 11.8 at.%. The values of the surface (Sn+Ca)/P molar ratios are close to the stoichiometric Ca/P molar ratio of HAP (1.67) for the samples at low Sn loading (Sn2.5/HAP, Sn5/HAP, and Sn7.5/HAP); this might suggest that the introduction of small amount of Sn on HAP would result in a partial exchange between Ca(II) and Sn(II) ions at the surface layers. Conversely, further addition of Sn (Sn loading ≥ 10 wt.%, Sn10/HAP, Sn12.5/HAP, and Sn15/HAP) causes a significant increase of (Sn+Ca)/P ratio up to a value of ca. 2, which indicates a surface enrichment of Sn phase covering HAP surface.

277 **Table 1.** *Bulk and surface composition of Sn/HAP samples*

Sample code	Sn content (wt.%)	Surface composition (XPS)					
		Sn (at.%)	O (at.%)	C (at.%)	Ca (at.%)	P (at.%)	(Sn+Ca)/P
Sn2.5/HAP	1.81 ± 0.04	1.5	63.4	1.7	20.1	13.3	1.62
Sn5/HAP	3.41 ± 0.03	1.6	62.8	1.8	20.2	13.5	1.62
Sn7.5/HAP	7.72 ± 0.07	4.4	63.6	0.7	18.4	12.8	1.77
Sn10/HAP	13.04 ± 0.08	7.6	62.8	1.1	16.0	12.5	1.88
Sn12.5/HAP	15.39 ± 0.08	11.5	62.9	1.8	12.6	11.2	2.14
Sn15/HAP	18.22 ± 0.08	11.8	62.5	1.0	12.6	12.1	2.01

278

279 Structural and morphological characterization was performed to assess the effect of Sn
280 deposition on the textural properties of hydroxyapatite.

281 X-ray diffraction (XRD) patterns of bare HAP, Sn7.5/HAP and Sn15/HAP are shown in
282 Figure 1, panel b. A comparative view demonstrates that the deposition of Sn onto HAP
283 surface did not alter the crystalline structure of the HAP. Indeed, in all the reported patterns,
284 the most intense diffraction peaks at 2θ values of 25.90°, 31.86°, 32.20°, 32.90°, 34.22°,
285 39.86°, 46.69° and 49.51° are consistent with the (002), (211), (112), (300), (202), (310),
286 (222) and (213) crystal planes of hydroxyapatite with hexagonal structure (JCPDS: 00-009-
287 0432). Moreover, no additional peaks ascribable to any segregated Sn-containing crystal
288 phase are detected even at high Sn loading (15 wt.%).

289 Transmission electron microscopy (TEM) images of bare HAP and Sn2.5/HAP, Sn7.5/HAP
290 and Sn12.5/HAP samples are reported in Figure 1 (panels c, d, e and f). TEM characterization
291 demonstrated that the peculiar needle-shaped morphology of synthetic HAP (Figure 1c) was
292 maintained after the addition of Sn (Figure 1d, 1e and 1f). In all micrographs, agglomerations
293 of elongated nanorods with sizes ranging between 50 – 200 nm in length and 6-8 nm in
294 width are present, with no evident difference in particles sizes and shape, apart from a
295 negligible aggregation for the sample with high Sn content (Sn12.5/HAP in Figure 1f).

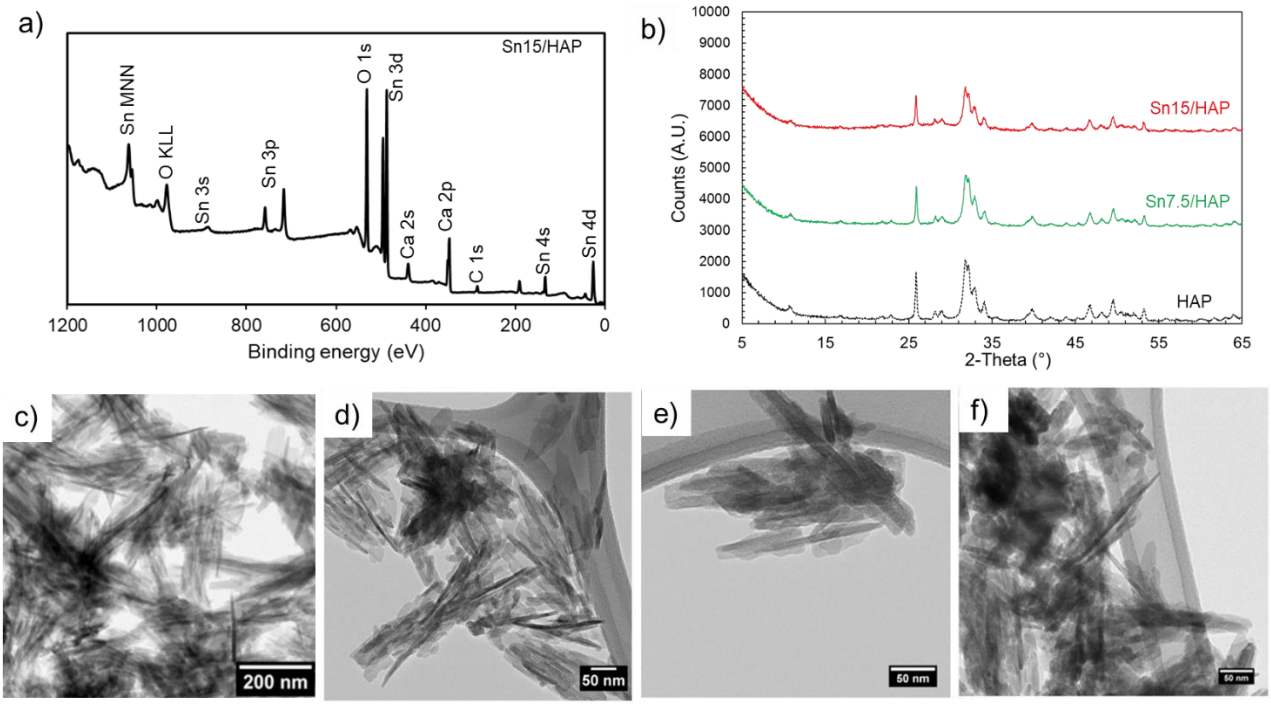

Figure 1 Morphological and structural characterization of Sn/HAP materials. a) XPS survey spectrum of Sn15/HAP; b) XRD patterns of bare HAP, Sn7.5/HAP and Sn15/HAP; TEM images of c) bare HAP, d) Sn2.5/HAP, e) Sn7.5/HAP and f) Sn12.5/HAP.

HAADF-STEM with elemental EDX maps in Figure S.1 show, as expected, the presence of Ca, P and Sn elements. Interestingly, a homogeneous Sn dispersion was achieved on the three samples (Sn2.5/HAP, Sn7.5/HAP, Sn12/HAP), with only minor segregation of Sn-phase, which appears as bright zone in Sn7.5/HAP (Fig. S.1b) and Sn12.5/HAP (Fig. S.1c).

The BET specific surface area, average pore diameter and average pore volume were determined by collecting the N_2 adsorption-desorption curves at 77 K (Figure S.2). Bare HAP sample exhibited a type IV profile according to IUPAC classification, associated with mesoporous materials. The desorption hysteresis, according to the de Boer's classification, is of type H2, typical of disordered materials with a not well-defined distribution of pore size and shape. The Brunauer-Emmett-Teller (B.E.T.) surface area and porosity values (Table S.1), confirmed that the prepared HAP is a mesoporous solid, with a specific surface area of ca. 78 $m^2 \cdot g^{-1}$ and mean pore radius of 5.5 nm. The deposition of tin on HAP up to 7.5 wt.% did not affect the surface area and pore size, which were found to be *ca.* 80 $m^2 \cdot g^{-1}$ and 6 nm, respectively. Conversely, for higher tin content (Sn ≥ 12.5 wt%), a decrease of the surface

area of ca. 25% was observed (59 $m^2 \cdot g^{-1}$); this could be ascribed to the formation of Sn aggregates, as suggested by STEM-EDX analysis.

3.2 Batch reductive adsorption studies

3.2.1. Influence of tin loading and initial Cr(VI) concentration

The effect of tin loading on the Cr(VI) removal capacity was investigated at different Cr(VI) initial concentration. As reported in the literature, Cr(VI) concentration in non-treated industrial wastewaters can be estimated to be in the range between 0.1 and 200 ppm, depending on the specific industrial source. Hence, in this study Cr(VI) aqueous solutions with initial concentrations ranging from 50 to 120 ppm were prepared from $K_2Cr_2O_7$. The prepared bichromate solutions were then contacted with Sn/HAP samples with different tin content to evaluate the performance of the samples. The values of pH (ca. 2), dosage (4.5 g L^{-1}), temperature (313 K) and contact time (4 h) did not change within this series of experiments. Figure 2 compares Cr(VI) removal capacity values (expressed as $mg_{Cr}\ g^{-1}$) of Sn/HAP materials for variable initial Cr(VI) concentrations.

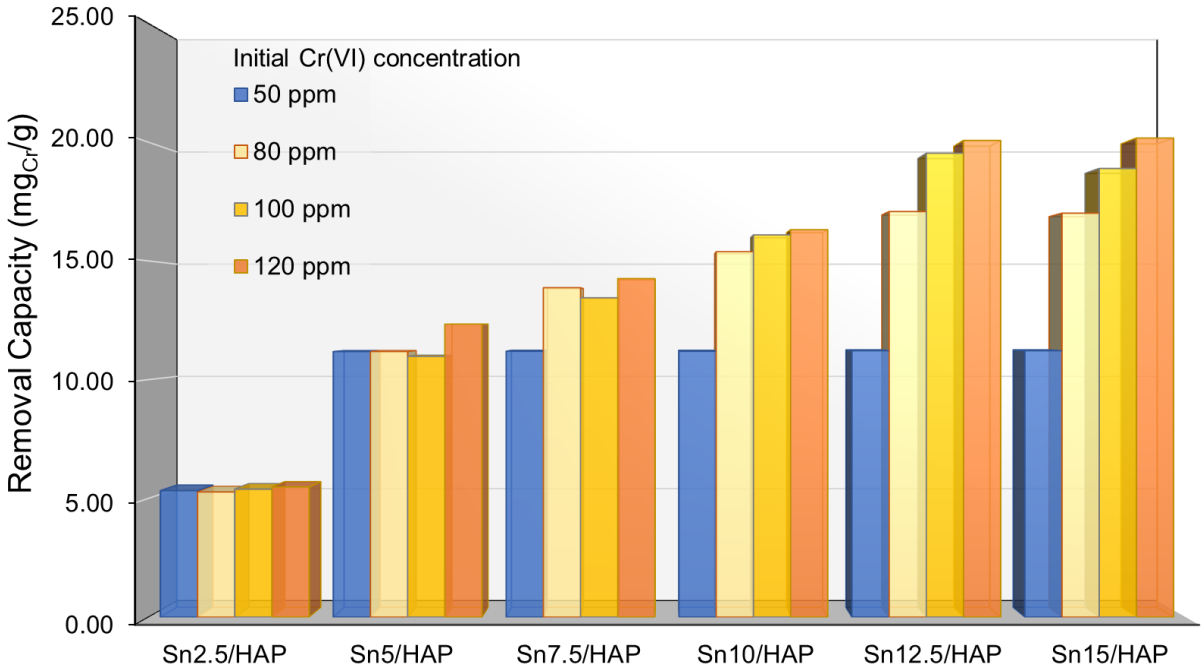

Figure 2. Results of Cr(VI) reduction-immobilization; effect of tin loading and initial Cr(VI) concentration. Operating conditions: pH = 2, dosage = 4.5 g L^{-1}, T = 313 K, t = 4 h

The Cr removal capacity was stable around constant values of approximatively 5 and 11 $mg_{Cr} \cdot g^{-1}$, respectively, for the samples with low Sn loading (Sn2.5/HAP and Sn5/HAP), independently on the initial Cr(VI) concentration. Considering the ratio between the molar amount of Sn present on these samples and the corresponding moles of Cr immobilized after the tests, values close to 1.5 are obtained. This value reflects the reaction stoichiometry of the redox reaction between Sn(II) and Cr(VI) described in equation 3:

$$3\,Sn^{2+} + Cr_2O_7{}^{2-} + 14\,H^+ \rightarrow 3\,Sn^{4+} + 2\,Cr^{3+} + 7\,H_2O \qquad E^0{}_{cell} = +1.18\ V \qquad (3)$$

$$\Delta G^0 = -zFE^0{}_{cell} = -683.12\ kJ\ mol^{-1}$$

Indeed, according to equation 3, 1.5 moles of tin are required per mole of hexavalent chromium to be reduced. It is then reasonable to suppose that in Sn2.5/HAP and Sn5/HAP samples almost all Sn is exposed at the surface and accessible for Cr(VI) reduction reaction which proceeds to the extent that there is still Sn available to react.

Increasing tin loading, the effect of the initial Cr(VI) concentration becomes evident. As a general trend, on all samples, the Cr(VI) removal capacity increased gradually with increasing Cr(VI) initial concentration up to reaching a ceiling value, which was greater the higher the Sn loading was in the sample up to Sn12.5/HAP sample. On the latter a maximum total Cr removal of ca. 20 $mg_{Cr}\ g^{-1}$ was attained. Further increase in tin loading (Sn15/HAP) did not produce any enhancement in the Cr(VI) removal capacity. The removal efficiency seems to be limited by the capacity of HAP in highly dispersing the deposited Sn(II)-phase. Indeed, increasing Sn loading, a partial aggregation may occur and only a fraction of tin is exposed at the surface available to react with Cr(VI).

In agreement with the observed results, plotting the Cr(VI) removal capacity as a function of surface tin concentration a linear trend was obtained on the samples with Sn loading higher than 2.5wt.% (Fig.3), thus confirming that tin dispersion at the surface of HAP is a key-parameter which directs the performance of the Sn/HAP samples.

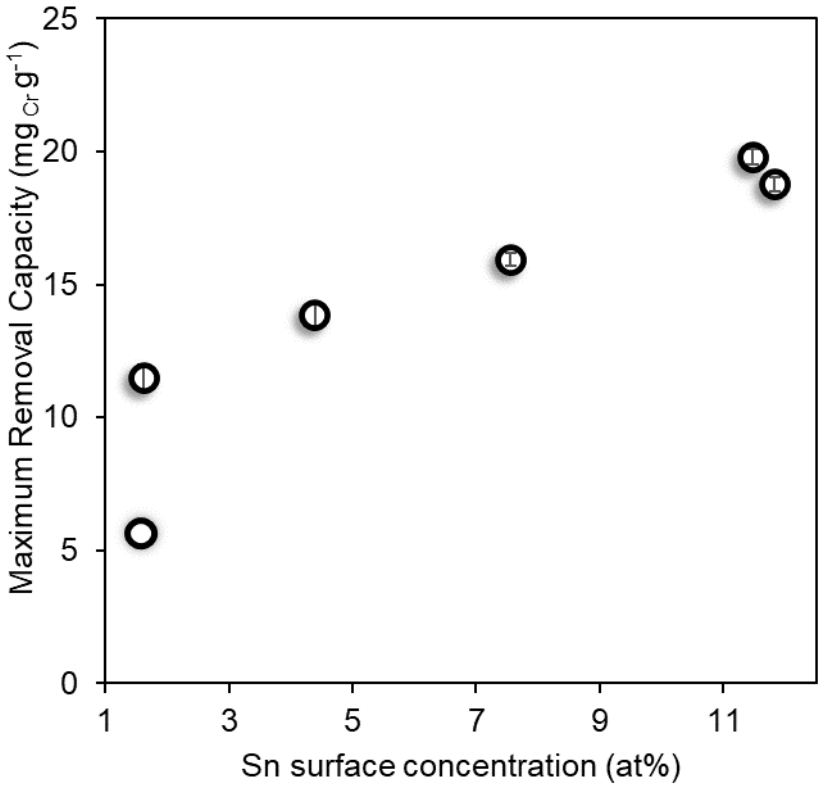

Figure 3. Relationship between the maximum Cr(VI) removal capacity and the surface concentration of tin in Sn/HAP materials.

On Sn12.5/HAP sample, a sort of reaction isotherm was collected at 313K plotting the equilibrium Cr removal capacity (q_e, mg_{Cr} g^{-1}) as a function of Cr(VI) residual concentration at equilibrium (Figure S.3). A sharp inflection was observed in the isotherm at very low values of equilibrium concentration, then a ceiling value was asymptotically approached, indicating the saturation of the surface with the Cr(VI) species. This isotherm profile was well fitted by the Langmuir model equation and a maximum removal capacity of 20.2 ± 0.6 mg_{Cr} g^{-1} was derived. This value corresponds to twice the previously reported value (10 mg_{Cr} g^{-1}) for Sn/HAP materials prepared by depositing $SnCl_2$ on a commercial hydroxyapatite (with low surface area) and tested under the same conditions [49]. A similar removal capacity was obtained by Asimakidou et al. using tin oxyhydroxide-decorated biochar with 20wt.% in tin phase [37]. These results confirm the important role of hydroxyapatite support in dispersing the tin phase.

3.2.2. Effect of pH and counter-cations

The effect of pH on Cr(VI) reductive adsorption from aqueous solution by Sn/HAP samples is shown in Fig. 4a, where the adsorption capacity as a function of tin loading is plotted for experiments carried out at pH = 2, 6, and 9.

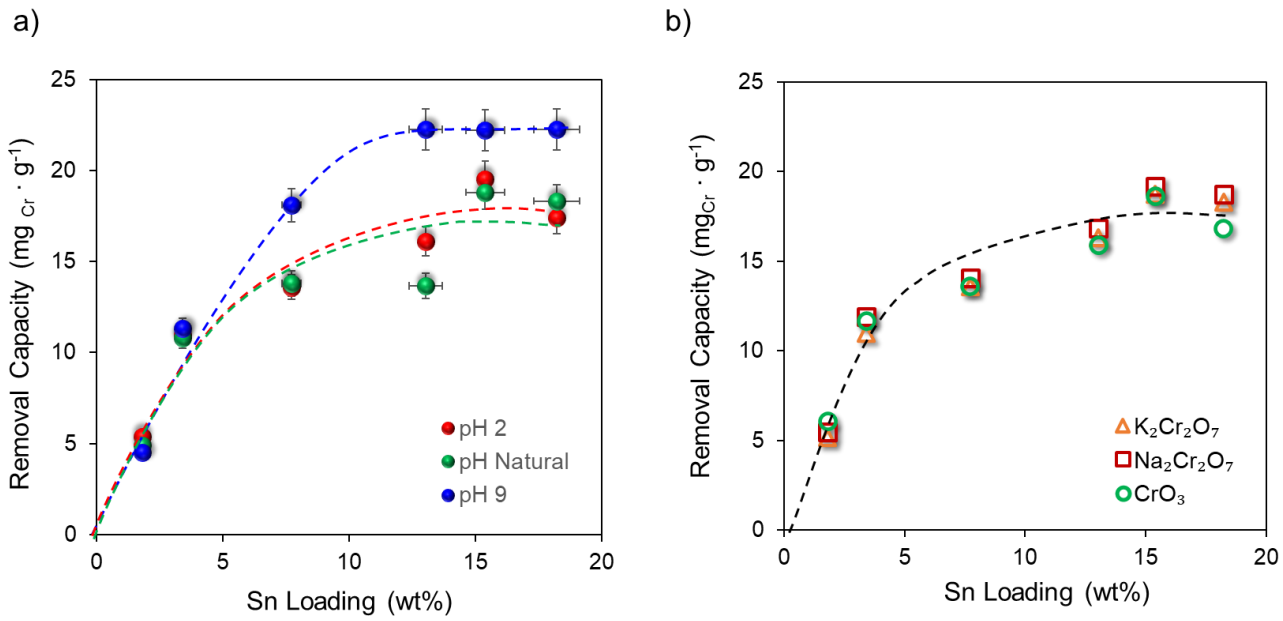

Figure 4. a) Effect of pH and b) effect of Cr(VI) precursor for the reductive adsorption of Cr(VI) on different Sn(II) loaded HAP samples . Experimental conditions: $[Cr(VI)]^{\circ}$ = 100 ppm, dosage = 4.5 g L^{-1}, T = 313 K, t = 4 h

Tests performed at pH 2 and 6 showed no significant differences in terms of Sn/HAP performance. This result is of paramount importance from an applicative point of view, since a pH value of 6 is very close to the natural pH imposed by HAP in solution. Thus, it seems that the intrinsic amphoteric character of HAP surface could be enough to ensure an effective Cr(VI) reduction, thus making unnecessary the use of acidic conditions, which can be deleterious for the stability of HAP at long contact time.

Interestingly, an increase of ca. 25% in Cr(VI) removal capacity was observed at pH 9 in experiments with Sn/HAP samples with tin loading higher than 7.5 wt%. This evidence finds adequate support in prior knowledge on homogenous Cr(VI) reduction by inorganic salts. Indeed, it is known that the redox potentials are affected by pH and in the case of Cr(VI)/Cr(III) and Sn(IV)/Sn(II), the standard potential values at basic pH are – 0.12 V and

392 – 0.96 V, respectively [36]. Thus, tin(II) species can act as strong reducing species towards
393 Cr(VI) even at pH = 9. In addition, looking at the Cr-speciation diagrams, at basic pH values,
394 Sn(II) is prevalently present as hydroxylated $[Sn(OH)_2]$ and $[Sn(OH)]^+$ species, which are
395 proposed to facilitate electron transfer, thanks to the presence of electron-donating OH^-
396 ligands [59]. In the case of Sn/HAP materials, at basic pH such hydroxylated species might
397 be formed at the interface, thus promoting Cr(VI) reduction. Furthermore, these species
398 might be leached from the HAP surface, thus causing the reduction to occur in homogeneous
399 phase.
400 The effect of the Cr(VI) precursor, and specifically of the counter-cation (Na^+, K^+ or H^+), was
401 investigated by preparing and testing three different solutions, with equal Cr(VI)
402 concentration of *ca.* 100 ppm, starting from three different chromium(VI) sources: $K_2Cr_2O_7$,
403 $Na_2Cr_2O_7$ and CrO_3 (the latter generating chromic acid, $HCrO_4$, once dissolved in water).
404 The counter-cations could influence the Cr(VI) removal performances, by modifying the
405 electric properties of the interface or by competing with Cr(III) cations for the adsorption
406 onto HAP surface.
407 However, the results shown in Fig. 4b demonstrate that the reductive adsorption capacity of
408 Sn/HAP materials are not affected by the nature of the counter-cation.

409 3.2.3 Effect of dosage and ageing

410 The effect of Sn/HAP dosage on the removal of Cr(VI) from aqueous solution at
411 concentration of ca. 100 ppm is shown in Fig. 5. Sn7.5/HAP was selected as representative
412 sample of the Sn/HAP series. As expected, the removal efficiency raised under an increasing
413 dosage.
414 The removal efficiency decreased from 60.8% to 13.2% and 9.4% with a decrease in dosage
415 from 4.5 g L^{-1} to 1 and 0.5 g L^{-1} respectively, as a consequence of the reduced availability of
416 sites for Cr(VI) reduction and Cr(III) adsorption. An enhancement in the removal efficiency

417 was observed when Sn/HAP dosage increased from 4.5 to 9 g L^{-1}. Indeed, an adsorbent
418 dosage of 9 g L^{-1} assured the complete removal of 100 ppm of Cr(VI) with an efficiency >99%.

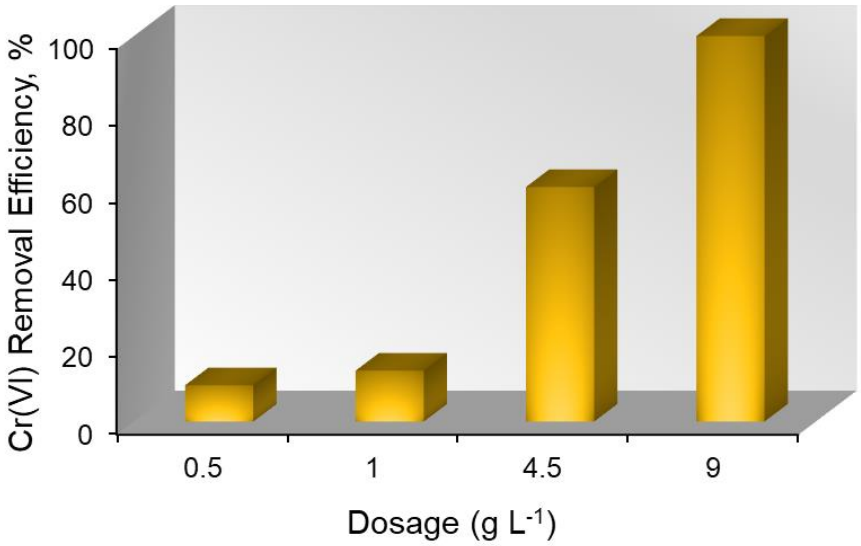

419

420 **Figure 5.** Effect of dosage in the reductive adsorption of Cr(VI). Experimental conditions: $[Cr(VI)]^{o}$ = 100
421 ppm, pH = 2, T = 313 K, and t= 4 h.

422 The effect of ageing time was explored on Sn12.5/HAP sample. The material was prepared
423 and then tested after different ageing times. During the ageing, the material was kept sealed
424 in a plastic container under a static air atmosphere and protected from light. The results of
425 the Cr(VI) removal tests are represented in Figure S.4.
426 From Figure S.4 it could be observed that the reductive adsorption capacity of Sn12.5/HAP
427 decreased with time following a non-linear trend. A steep decrease of the performance was
428 observed after the first 3 weeks, when the Cr(VI) removal efficiency dropped from an initial
429 85% to 58%, corresponding to a decrease of ca. 30%, whereas only a moderate decrease was
430 observed after 85 days, with an overall 50% loss of activity.

431 3.2.4. Kinetics and thermodynamics insights

432 The kinetics of the Cr(VI) reductive adsorption process on Sn/HAP materials was studied
433 selecting Sn7.5/HAP as representative sample. Residual Cr(VI) concentration versus time
434 (Fig. 6a) and Cr uptake versus time (Fig. 6b) curves were collected, upon contacting

435 Sn7.5/HAP with a 100 ppm Cr(VI) solution at pH 2 and 313 K. Experimental profiles
436 showed that Cr(VI) concentration exponentially decreased with a rapid drop within the first
437 200-300 min.

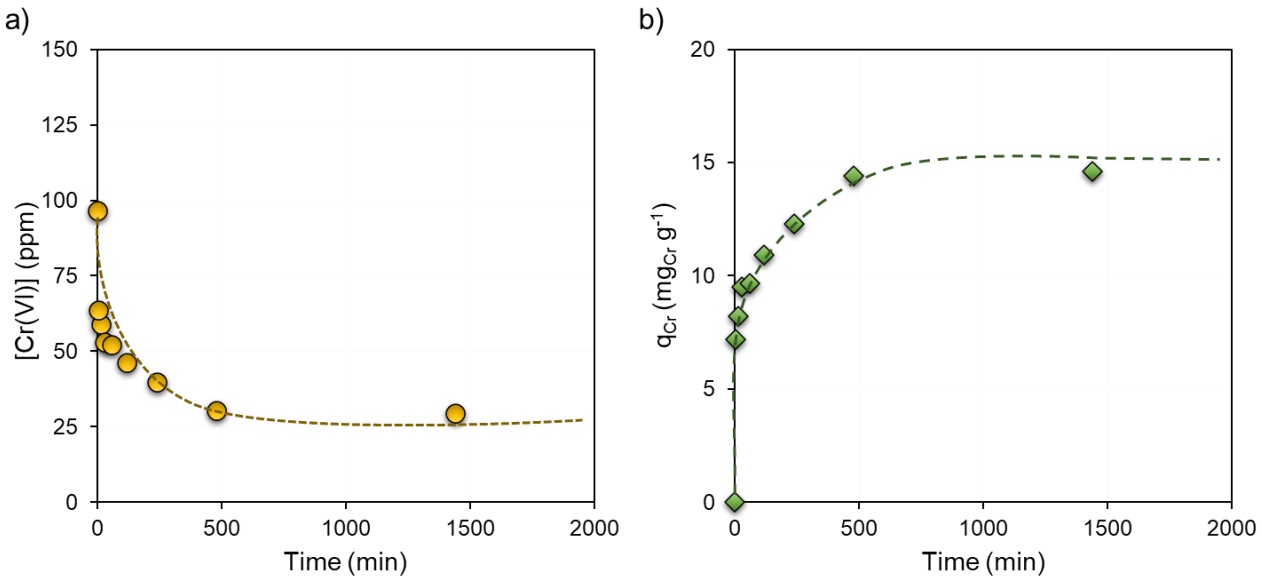

438

439 **Figure 6.** Kinetic profiles of Sn7.5/HAP at 313 K, in terms of a) Cr(VI) concentration and b) Cr uptake (right)
440 as a function of time.

441 The kinetics curves of Cr(VI) reductive adsorption was analysed using three empirical
442 models: pseudo-first order (PFO), pseudo-second order (PSO) and Elovich models (Table
443 S.2) [60]. The kinetic parameters were calculated for the three kinetic models, by linear least
444 square method, starting from the integrated linearized equations. The rate constants along
445 with the relative regression coefficients are reported in Table 2 (the linear regression curves
446 are reported in Fig. S.5).

447 **Table 2**. Kinetic parameters obtained for the Cr(VI) reductive adsorption on Sn7.5/HAP sample

PFO model			PSO model			Elovich		
k_1 (1/min)	$q_{e,cal}$ [b] (mg/g)	R^2	k_2 (g/mg min)	$q_{e,cal}$ [b] (mg/g)	R^2	a (mg/g min)	b (g/mg)	R^2
$5.5 \cdot 10^{-3} \pm 0.1 \cdot 10^{-3}$	6.9	0.889	$1.7 \cdot 10^{-2} \pm 7 \cdot 10^{-3}$	11.2±0.4	0.996	107.9±1.2	0.86±0.04	0.968

448 [a] Cr(VI) adsorption capacity at equilibrium obtained with PFO and PSO model by fitting the experimental data.

From the results obtained, it can be concluded that the time-dependency of Cr(VI) reductive adsorption is well described by the pseudo-second-order model with a calculated rate constant of $1.7 \cdot 10^{-2}$ g·mg^{-1}·min^{-1}.

On Sn7.5/HAP sample, the kinetic tests were carried at different temperatures (278, 288, 298, 308 and 318 K) by using 100 ppm Cr(VI) solutions at pH 2 and dosage 4.5 g L^{-1},

The apparent rate constant values at 278, 288, 298, 308 and 318 K, respectively, are gathered in Table S.3. The reaction rate shows a clear exponentially increasing trend of the reaction rate with temperature (Fig. S.6a). The plot of the logarithm of the apparent rate constants ($\ln k_{obs}$) versus the inverse temperature (1/T) gives a negatively-sloped straight line (Fig. S.6b), which was linearly fitted to extrapolate the pre-exponential factor (A) and the activation energy (E_a) values (Table S.3). Usually small activation energy values (< ca. 4 kJ mol^{-1}) are associated with physical adsorption involving weak interaction forces between adsorbate and adsorbent. In this case, the obtained activation energy value (21.3±0.6 kJ mol^{-1}) is significantly higher than that expected for physisorption, indicating that the Cr(VI) removal process is not a mere adsorption and thus confirming the reductive adsorption mechanism.

The reductive adsorption of Cr(VI) onto Sn/HAP can be considered as an equilibrium process described by the following equation:

$$Cr(VI)_{(aq)} + Sn(II)_{(HAPsurf)} \rightleftharpoons Cr(III)_{(HAPsurf)} + Sn(IV)_{(HAPsurf)} \quad (4)$$

A thermodynamic equilibrium constant can be defined as the ratio between the equilibrium Cr(VI) amount onto Sn/HAP (q_{eq}) and the residual concentration of Cr(VI) in solution at equilibrium (C_{eq}).

$$K = \frac{q_{eq}}{C_{eq}} \quad (5)$$

The temperature is expected to influence the equilibrium and the thermodynamics of the process. To investigate such an effect, the main thermodynamic parameters, i.e. standard Gibbs free energy change (ΔG°), standard enthalpy change (ΔH°) and standard entropy change (ΔS°) were computed from the variation of the thermodynamic equilibrium constant, K_T, with temperatures. At each temperature, the standard free energy change was determined according to Eq. (6).

$$\Delta G^\circ = -RT\ lnK \quad (6)$$

where R (8.314 J mol^{-1} K^{-1}) is the universal gas constant, T (K) is the temperature, and K is the equilibrium constant.

The values of ΔH° and ΔS° were obtained from the slope and intercept, respectively, of the van't Hoff plot (lnK versus 1/T), as shown in Figure S.7. The obtained thermodynamic data are gathered in Table 3. The negative Gibbs free energy change values validated the feasibility and spontaneity of the process. The reductive adsorption resulted to be an endothermic process with a positive enthalpy change value (ΔH°=+11.8 kJ mol^{-1}). The positive value of entropy change (+85.1 J mol^{-1} K^{-1}) could be ascribed to an increased randomness and structural rearrangements at the solid–aqueous solution interface during the process.

Table 3. Thermodynamic data for reductive adsorption of Cr(VI) at pH 2.

Sample Code	Temperature (K)	ΔG° (kJ mol^{-1})	ΔH° (kJ mol^{-1})	ΔS° (J $mol^{-1}K^{-1}$)
Sn7.5/HAP	278 ± 0.1	-12.0	+11.8 ±0.1	+94.8 ±0.9
	288 ± 0.1	-12.6		
	298 ± 0.1	-13.5		
	308 ± 0.1	-14.3		
	318 ± 0.1	-15.5		

3.2.5. Regeneration and characterization of used adsorbents

Adsorbent reusability studies were carried out to investigate the potential of the re-use of used Sn/HAP without any regenerative treatment for successive Cr(VI) removal tests. The Cr(VI) removal efficiency dramatically decreased during successive cycles of Sn7.5/HAP. Indeed, compared to the first removal capacity (10.8 ± 0.1 mg/g), the regenerated capacity in the second and third cycles (0.8 ± 0.2 mg/g) decreased by more than 95%. To regenerate the used Sn+Cr/HAP material in Cr(VI) reductive adsorption process, the liquid phase reduction with hydroxylamine hydrochloride and the gas phase reduction under hydrogen atmosphere were attempted. Unfortunately, both the regeneration methods were not able to restore even partially the pristine Sn/HAP activity (Fig. S.8).

To deeply investigate the causes of such a lack in the regeneration of used Sn+Cr/HAP materials, targeted characterization was carried out on the recovered reductive adsorbents after use.

The results of N_2 adsorption/desorption analysis on Sn7.5+Cr/HAP, listed in Table S.1, showed that the surface area and porosity (78 $m^2\ g^{-1}$) were not affected by Cr(VI) reductive adsorption test at pH 2 and 313 K, highlighting the great stability of the HAP structure.

According to ICP analysis the tin loading was not altered after the use, confirming the stable anchoring of the Sn phase onto HAP (Table 4).

However, based on STEM-EDX (Fig. 7a) and XPS characterization, Cr(III) species might be supposed to be adsorbed onto HAP in close proximity of the Sn centres, thus partially covering them and then hindering their accessibility to the reducing agents.

Indeed, HAADF-STEM and EDX analyses on used Sn7.5/HAP sample in Cr(VI) reduction-adsorption processes (Sn7.5+Cr/HAP) confirmed that the pristine needle-shape morphology was retained, without significant size variations (Figure S.9). EDX analyses of the Sn7.5+Cr/HAP sample showed that the Sn aggregation was well maintained after use in Cr removal process (Fig. 7a). Interestingly also chromium is highly dispersed on Sn/HAP

surface, suggesting that Cr(III) species formed by reduction of Cr(VI) are immediately adsorbed and stably anchored at the surface of Sn/HAP materials.

Actually, XPS analysis (Table 4) revealed the presence of Cr in the surface layers. A slight decrease in the surface concentration of Sn from 4.4 to 2.8 was observed after use, likely due to the deposition of an outer layer of Cr, partially shielding the Sn phase. High resolution Cr 2p spectrum (Fig. 7c), showed the $2p_{1/2}$ and $2p_{3/2}$ doublet pair at 587.3 and 577.7 eV with a peak separation of 9.6 eV typical of the Cr(III) oxidation state. The absence of components ascribable to chromium in Cr(VI) oxidation state on the surface of spent Sn7.5/HAP corroborated the successful occurrence of reductive adsorption process.

Table 4 *Surface composition of used Sn7.5+Cr/HAP sample before and after calcination*

Sample code	Sn content (wt.%)	Surface composition (XPS)						
		Sn (at.%)	Cr (at.%)	O (at.%)	C (at.%)	Ca (at.%)	P (at.%)	(Sn+Ca)/P
Sn7.5+Cr/HAP	7.69 ± 0.04	2.8	1.1	62.9	1.1	18.4	13.6	1.55
Sn7.5+Cr/HAP calcined		2.9	1.4	63.3	1.5	17.5	13.4	1.52

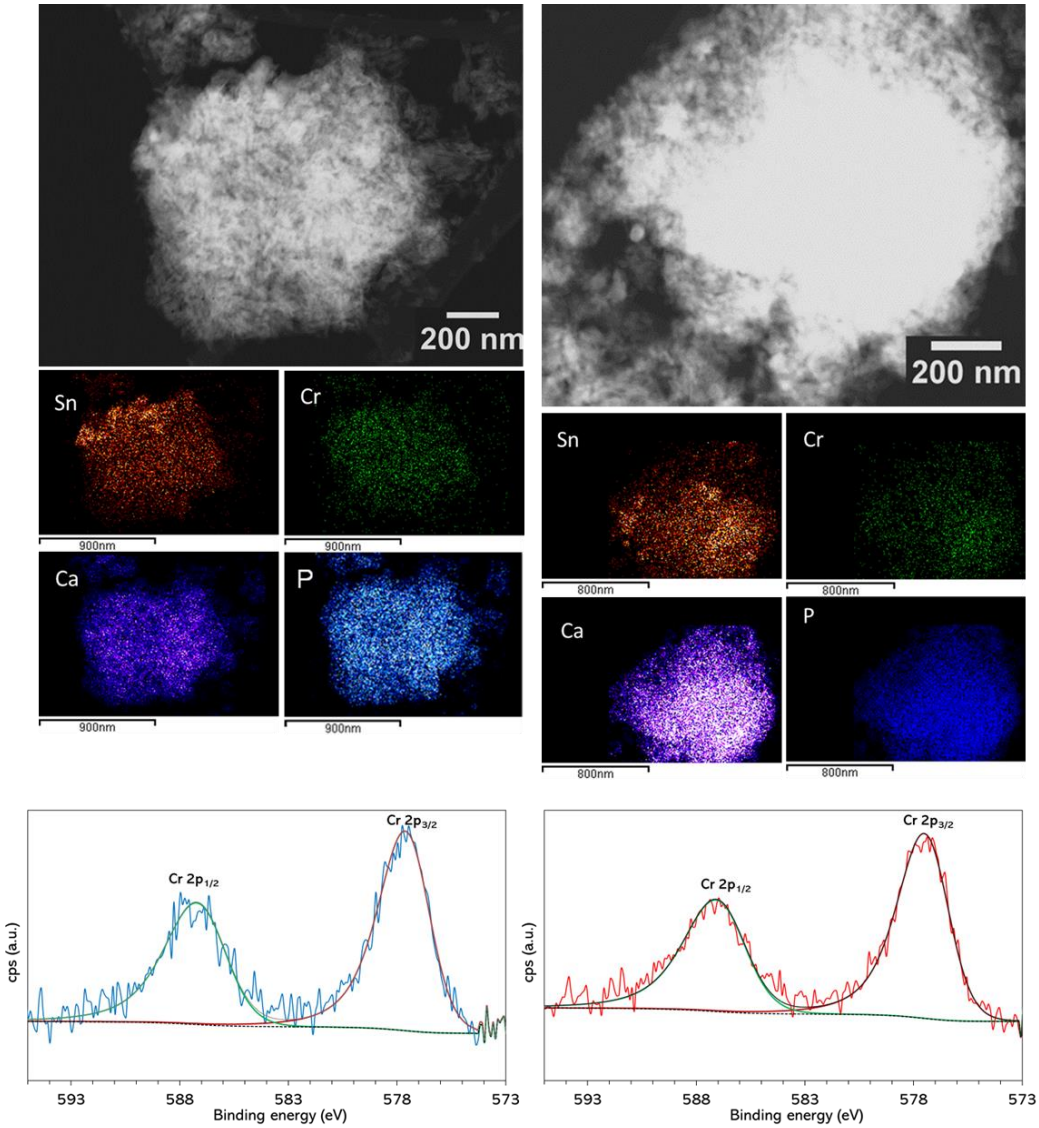

Figure 7. EDX compositional mapping analysis for Sn7.5+Cr/HAP a) before and b) after calcination (P is in blue, Ca in violet and Sn in orange) and HR Cr 2p spectra for Sn7.5+Cr/HAP c) before and d) after calcination.

3.3 Upcycling of used SnCr/HAP into environmental catalysts

The unsuccessful regeneration of the spent Sn+Cr/HAP materials poses a challenge since the disposal of the used adsorbents may produce secondary pollution and imply unsustainable costs. Therefore, the reuse of already used Sn+Cr/HAP adsorbents as catalysts has been here examined in the context of resource recovery and circular economy. In fact, both Sn- and Cr-containing phases are known to be highly active in acid and redox catalysis [62–64]. They have found successful application as active phases or modifiers in environmental catalysts for NO_x abatement[65–70]. Hydroxyapatite, as well, is attracting ever more attentions as ecofriendly and low-cost support for catalytic applications in several processes for air pollution mitigation (e.g. NO_x abatement, NH_3 selective oxidation, N_2O decomposition, CO_2 reduction reaction) [56,57,71,72]. Based on these premises, used Sn7.5+Cr/HAP sample was at first tested as catalysts in the selective catalytic reduction of NO_x by NH_3 (NH_3-SCR). This process is usually carried out at high temperatures, thus the recovered Sn7.5+Cr/HAP material was preliminarily stabilized by calcination at 773 K in air. This thermal treatment did not lead any significant change in the morphology and surface composition of the material, as proved by surface area measurements (Table S.1), STEM-EDX (Fig. 7b) and XPS analyses (Table 4). Interestingly, no Cr(VI) formation from Cr(III) oxidation at the surface was observed according to Cr 2p XP spectrum, despite the severe conditions adopted in the calcination step (Fig. 7c). The absence of Cr(VI) species is vital for a safe management of the calcined materials, considering the toxicity of Cr(VI).

3.3.1. Selective catalytic reduction of NO_x by NH_3 (NH_3-SCR)

The selective catalytic reduction of NO_x by NH_3 (NH_3-SCR) represents one of the most effective solutions for the abatement of NO_x emitted from both mobile and stationary sources. The process consists in the selective reduction of NO_x to N_2 by ammonia as reducing

561 agent and in the presence of a catalyst. The standard NH_3-SCR is described by the following
562 reaction:

563 $$4\,NH_3 + 4\,NO + O_2 \rightarrow 4\,N_2 + 6\,H_2O \quad (7)$$

564 In oxygen-rich mixtures and at high temperatures (> 600 K) parasite NH_3 oxidation by
565 oxygen depresses the selectivity of the process and led to an undesired formation of NO_x and
566 N_2O.
567 The catalytic behaviour of Sn7.5+Cr/HAP was studied in the NH_3-SCR reaction in the
568 temperature range between 393 and 773 K, at fixed gas hourly space velocity (GHSV) of ca.
569 40000 h^{-1} and with NH_3 and NO initial concentrations of ca. 500 ppm each. As reported in
570 Figure S.10 which plots the conversion and selectivity profiles of fed and formed species,
571 respectively, as a function of the temperature, Sn7.5+Cr/HAP samples was able to convert
572 NO starting from 523 K and attained a maximum NO conversion value of ca. 50% at 623 K.
573 The performance of Sn7.5+Cr/HAP matches that of a physical mixture of tin dioxide,
574 manganese oxide and beta zeolite in NO_x reduction by propane, as reported by Corma et al.
575 [66], although a direct comparison is far from trivial. Concerning the selectivity, a quite low
576 selectivity to N_2 was observed throughout the investigated temperature range over
577 Sn7.5+Cr/HAP, due to the formation of large quantities of N_2O. Low selectivity to N_2 and
578 preferential formation of N_2O were observed also by Shi et al. over Sn modified Cr-MnO_x
579 catalysts [70].
580 These results evidenced the prominent oxidizing capacity of Sn- and Cr-containing
581 hydroxyapatites and encouraged to test the catalytic performance of the Sn7.5+Cr/HAP in
582 two catalytic oxidation processes of environmental relevance, i.e. the the selective catalytic
583 oxidation of NH_3 (NH_3-SCO) and the selective catalytic oxidation of methane to CO_2
584

585

3.3.2. Selective catalytic oxidation of NH_3 (NH_3-SCO)

Selective catalytic oxidation (SCO) is considered as one of the most effective technology to face ammonia slipping problem in oxygen-containing gaseous effluents [73]. In the NH_3-SCO ammonia is converted into N_2, according to the following reaction:

$$4NH_3 + 3O_2 \rightarrow 2N_2 + 6H_2O \quad (8)$$

An effective catalyst should be able to selectively convert NH_3, present at extremely low concentration, into N_2, preventing further oxidation to the undesired NO_x and N_2O.

NH_3-SCO tests were performed with Sn7.5+Cr/HAP with the aim of investigating their catalytic activity in the temperature range between 393 and 773 K (see Experimental section).

The results indicate that efficient NH_3 conversion can be achieved over Sn7.5+Cr/HAP, with catalytic activity starting at 473 K and reaching 90% conversion at 673 K (Figure S.10) in line with conventional metal-doped zeolite catalysts [73]. However, the selectivity to N_2 was quite low and it maintained around a constant value of 30% in the 523 – 673 K range, where N_2O formation was favored. Above 673 K, the selectivity to N_2O decreased, and a significative formation of NO was observed. These outcomes confirmed the pronounced oxidizing ability of Sn7.5+Cr/HAP surface.

3.3.3. Selective catalytic oxidation of CH_4

Methane (CH_4), the main component of natural gas, is known to be a greenhouse gas with warming effect about 25 times that of CO_2. The direct oxidation to CO_2 and water represents the most common after-treatment technology for the abatement of unconverted methane vented from the power plant, vehicle and chemical industries using natural gas as energy source. Due to the extremely high thermodynamic stability of CH_4, high temperatures are required for the direct combustion of methane, leading to the formation of toxic secondary products (e.g. NOx). The use of a catalyst has a beneficial effect on the process, allowing to

operate at low temperatures. The catalytic activity of Sn7.5+Cr/HAP in methane oxidation was investigated in the temperature interval between 573 and 1033 K, at a fixed GHSV of ca. 60000 h^{-1} and with an initial CH_4 concentration of ca. 1500 ppm and an excess of O_2 (ca. 30000 ppm). The catalyst was inactive in methane oxidation below 723 K, then CH_4 conversion gradually increased up to ca. 30% at 1023 K. The attained methane conversion, while still not high, is a remarkable result, if related to the small amount of Sn and Cr present in the catalyst (7.5wt.% and 1.5wt.%, respectively). Actually, the specific activity at 650°C (calculated as ppm of converted methane per unit of time and mass of chromium) has a value of $1.69 \cdot 10^{-5}$ ppm min^{-1} g_{Cr}^{-1}, which is slightly higher than that reported in the literature for supported copper chromite with Cr content of 7.7wt.% ($1.25 \cdot 10^{-5}$ ppm min^{-1} g_{Cr}^{-1})[74]. Concerning the selectivity, in the whole range of temperature only CO_2 and H_2O were detected as products (Figure 8).

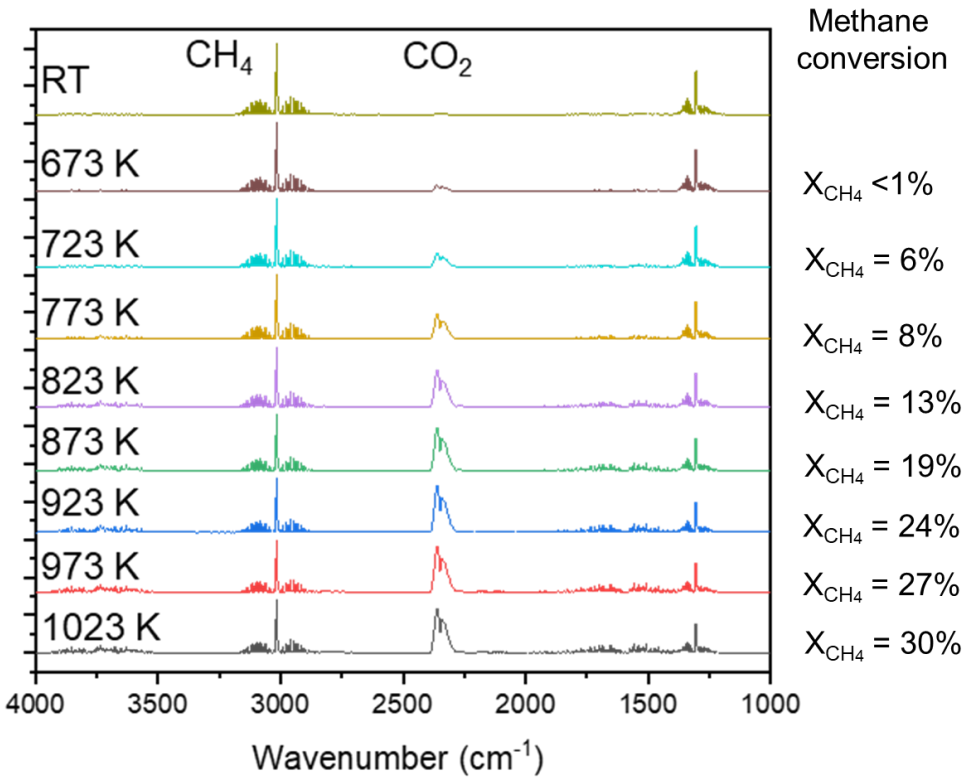

Figure 8. FTIR spectra recorded during methane oxidation over Sn7.5+Cr/HAP catalyst

Although noble metal catalysts (Pd, Pt) are able to activate C–H bond and to completely convert methane at significantly lower temperatures than Sn7.5+Cr/HAP, their use is definitely less advantageous from an economic point of view. It should be also noted that CH_4 molecule is more stable than other hydrocarbons and organic substrates, thus the obtained results are particularly promising in the light of a possible application of the used adsorbents in the catalytic abatement of other organic air-contaminants, such as volatile organic compounds.

Conclusions

In conclusion, Sn-modified hydroxyapatite (Sn/HAP) materials with improved tin dispersion and promising performance in the reductive adsorption of Cr(VI) have been successfully prepared. The Cr(VI) removal efficiency of Sn/HAP materials was mainly governed by the surface Sn concentration. Indeed, Sn/HAP materials (Sn12.5/HAP and Sn15/HAP) with the highest Sn surface concentration exhibited the best performance. The removal capacity of Sn12.5/HAP for Cr(VI) at temperature of 313 K was ca. 20 mg_{Cr}/g, which was 2 time-fold higher than that of other Sn-based reductive adsorbents already presented in the literature. The removal of Cr(VI) by reductive adsorption mechanism was spontaneous in nature and took place with a fast kinetics well described by pseudo-second order model. Characterization using XPS and HAADF-STEM-EDX showed that Cr was highly dispersed as Cr(III) onto the surface of Sn/HAP materials after their utilization to remove Cr(VI), confirming that the Cr(VI) removal consisted in a reduction process accompanied by adsorption of formed Cr(III). The presence of Cr(III) phase in the surface layers partially hindered the accessibility of Sn centers, making difficult the regeneration by reductive agents for the reuse of used adsorbents. An “adsorbent-to-catalyst” upcycling approach was then used in this study. The used adsorbents were tested as catalysts in selected environmental reactions for air-contaminant abatement. The upcycled adsorbents demonstrated to possess a marked oxidizing capacity that could be exploited in selective

total oxidation processes, such as VOC combustion. If properly optimized and improved, this strategy could assure simultaneous mitigation of both water and air pollution and have great potential for practical implementation, resulting in in cost-effectiveness, sustainable waste management and resource recovery.

Acknowledgement

This work was partially supported by the grant INAIL BRIC 2018-2019 ID13.

References

[1] H. Karimi-Maleh, A. Ayati, S. Ghanbari, Y. Orooji, B. Tanhaei, F. Karimi, M. Alizadeh, J. Rouhi, L. Fu, M. Sillanpää, Recent advances in removal techniques of Cr(VI) toxic ion from aqueous solution: A comprehensive review, J. Mol. Liq. 329 (2021). https://doi.org/10.1016/j.molliq.2020.115062.

[2] N. Sharma, K.K. Sodhi, M. Kumar, D.K. Singh, Heavy metal pollution: Insights into chromium eco-toxicity and recent advancement in its remediation, Environ. Nanotechnology, Monit. Manag. 15 (2021) 100388. https://doi.org/10.1016/j.enmm.2020.100388.

[3] M. Tumolo, V. Ancona, D. De Paola, D. Losacco, C. Campanale, C. Massarelli, V.F. Uricchio, Chromium pollution in European water, sources, health risk, and remediation strategies: An overview, Int. J. Environ. Res. Public Health. 17 (2020) 1–25. https://doi.org/10.3390/ijerph17155438.

[4] V.E. Pakade, N.T. Tavengwa, L.M. Madikizela, Recent advances in hexavalent chromium removal from aqueous solutions by adsorptive methods, RSC Adv. 9 (2019) 26142–26164. https://doi.org/10.1039/c9ra05188k.

[5] T. Lü, R. Ma, K. Ke, D. Zhang, D. Qi, H. Zhao, Synthesis of gallic acid functionalized magnetic hydrogel beads for enhanced synergistic reduction and adsorption of

aqueous chromium, Chem. Eng. J. 408 (2021). https://doi.org/10.1016/j.cej.2020.127327.

[6] W. Jiang, Q. Cai, W. Xu, M. Yang, Y. Cai, D.D. Dionysiou, K.E. O'Shea, Cr(VI) adsorption and reduction by humic acid coated on magnetite, Environ. Sci. Technol. 48 (2014) 8078–8085. https://doi.org/10.1021/es405804m.

[7] Y. Zhang, J. Yang, J. Du, B. Xing, Goethite catalyzed Cr(VI) reduction by tartaric acid via surface adsorption, Ecotoxicol. Environ. Saf. 171 (2019) 594–599. https://doi.org/10.1016/j.ecoenv.2019.01.024.

[8] J. Cao, Z. Cui, T. Wang, Q. Zou, Q. Zeng, S. Luo, Y. Liu, B. Liu, Reductive removal of Cr(VI) by citric acid promoted by ceramsite particles: Kinetics, influential factors, and mechanisms, Mater. Today Commun. 28 (2021) 102716. https://doi.org/10.1016/j.mtcomm.2021.102716.

[9] F. Liu, M. Xiang, A. Wang, C. Wang, B. Hu, Efficient adsorption and reduction of Cr(VI) and U(VI) by nanoscale zero-valent iron supported on polydopamine-decorated SBA-15, Appl. Surf. Sci. 568 (2021) 150931. https://doi.org/10.1016/j.apsusc.2021.150931.

[10] K.K. Krishnani, S. Srinives, B.C. Mohapatra, V.M. Boddu, J. Hao, X. Meng, A. Mulchandani, Hexavalent chromium removal mechanism using conducting polymers, J. Hazard. Mater. 252–253 (2013) 99–106. https://doi.org/10.1016/j.jhazmat.2013.01.079.

[11] B. Zuo, Q. Deng, H. Shao, B. Cao, Y. Fan, W. Li, M. Huang, Fe3O4@Mesoporous-SiO2@Chitosan@Polyaniline Core-Shell Nanoparticles as Recyclable Adsorbents and Reductants for Hexavalent Chromium, ACS Appl. Nano Mater. 4 (2021) 1831–1840. https://doi.org/10.1021/acsanm.0c03235.

[12] N.H. Kera, M. Bhaumik, K. Pillay, S.S. Ray, A. Maity, Selective removal of toxic Cr(VI) from aqueous solution by adsorption combined with reduction at a magnetic nanocomposite surface, J. Colloid Interface Sci. 503 (2017) 214–228. https://doi.org/10.1016/j.jcis.2017.05.018.

[13] B. Yao, M. Liu, Y. Gao, Y. Liu, S. Cong, D. Zou, Removal of hexavalent chromium in aqueous solution using organic iron-based composites synthesized and immobilized by natural dried willow leaves, J. Clean. Prod. 247 (2020) 119132. https://doi.org/10.1016/j.jclepro.2019.119132.

[14] M. Laabd, A. Imgharn, A. Hsini, Y. Naciri, M. Mobarak, S. Szunerits, R. Boukherroub, A. Albourine, Efficient detoxification of Cr(VI)-containing effluents by sequential adsorption and reduction using a novel cysteine-doped PANi@faujasite composite: Experimental study supported by advanced statistical physics prediction, J. Hazard. Mater. 422 (2022) 126857. https://doi.org/10.1016/j.jhazmat.2021.126857.

[15] M. Pettine, D. Tonnina, F.J. Millero, Chromium(VI) reduction by sulphur(IV) in aqueous solutions, Mar. Chem. 99 (2006) 31–41. https://doi.org/10.1016/j.marchem.2005.02.003.

[16] C. Kim, Q. Zhou, B. Deng, E.C. Thornton, H. Xu, Chromium(VI) Reduction by Hydrogen Sulfide in Aqueous Media: Stoichiometry and Kinetics, Environ. Sci. Technol. 35 (2001) 2219–2225. https://doi.org/10.1021/es0017007.

[17] W. Liu, L. Jin, J. Xu, J. Liu, Y. Li, P. Zhou, C. Wang, R.A. Dahlgren, X. Wang, Insight into pH dependent Cr(VI) removal with magnetic Fe3S4, Chem. Eng. J. 359 (2019) 564–571. https://doi.org/10.1016/j.cej.2018.11.192.

[18] W. Yang, D. Xi, C. Li, Z. Yang, Z. Lin, M. Si, “In-situ synthesized” iron-based bimetal

promotes efficient removal of Cr(VI) in by zero-valent iron-loaded hydroxyapatite, J. Hazard. Mater. 420 (2021) 126540. https://doi.org/10.1016/j.jhazmat.2021.126540.

[19] Y. Yang, Y. Zhang, G. Wang, Z. Yang, J. Xian, Y. Yang, T. Li, Y. Pu, Y. Jia, Y. Li, Z. Cheng, S. Zhang, X. Xu, Adsorption and reduction of Cr(VI) by a novel nanoscale FeS/chitosan/biochar composite from aqueous solution, J. Environ. Chem. Eng. 9 (2021) 105407. https://doi.org/10.1016/j.jece.2021.105407.

[20] Y. Fang, X. Wu, M. Dai, A. Lopez-Valdivieso, S. Raza, I. Ali, C. Peng, J. Li, I. Naz, The sequestration of aqueous Cr(VI) by zero valent iron-based materials: From synthesis to practical application, J. Clean. Prod. 312 (2021) 127678. https://doi.org/10.1016/j.jclepro.2021.127678.

[21] L. Yan, F.X. Dong, X. Lin, X.H. Zhou, L.J. Kong, W. Chu, Z.H. Diao, Insights into the removal of Cr(VI) by a biochar–iron composite from aqueous solution: Reactivity, kinetics and mechanism, Environ. Technol. Innov. 24 (2021) 102057. https://doi.org/10.1016/j.eti.2021.102057.

[22] F. Yang, Y. Jiang, M. Dai, X. Hou, C. Peng, Active biochar-supported iron oxides for Cr(VI) removal from groundwater: Kinetics, stability and the key role of FeO in electron-transfer mechanism, J. Hazard. Mater. 424 (2022) 127542. https://doi.org/10.1016/j.jhazmat.2021.127542.

[23] Y. Wang, Y. Gong, N. Lin, H. Jiang, X. Wei, N. Liu, X. Zhang, Cellulose hydrogel coated nanometer zero-valent iron intercalated montmorillonite (CH-MMT-nFe0) for enhanced reductive removal of Cr(VI): Characterization, performance, and mechanisms, J. Mol. Liq. 347 (2022) 118355. https://doi.org/10.1016/j.molliq.2021.118355.

[24] Q. Zhang, X. Ye, D. Chen, W. Xiao, S. Zhao, J. Li, H. Li, Chromium(VI) removal from

746 synthetic solution using novel zero-valent iron biochar composites derived from
747 iron-rich sludge via one-pot synthesis, J. Water Process Eng. 47 (2022) 102720.
748 https://doi.org/10.1016/j.jwpe.2022.102720.

749 [25] G. Gao, L. Zhang, Y. Shi, S. Yang, G. Wang, H. Xu, D. Ding, R. Chen, P. Jin, X.C.
750 Wang, Mutual-activation between Zero-Valent iron and graphitic carbon for Cr(VI)
751 Removal: Mechanism and inhibition of inherent Side-reaction, J. Colloid Interface
752 Sci. 608 (2022) 588–598. https://doi.org/10.1016/j.jcis.2021.09.138.

753 [26] Y. Liu, S.P. Sohi, S. Liu, J. Guan, J. Zhou, J. Chen, Adsorption and reductive
754 degradation of Cr(VI) and TCE by a simply synthesized zero valent iron magnetic
755 biochar, J. Environ. Manage. 235 (2019) 276–281.
756 https://doi.org/10.1016/j.jenvman.2019.01.045.

757 [27] Y. Qiu, Q. Zhang, B. Gao, M. Li, Z. Fan, W. Sang, H. Hao, X. Wei, Removal
758 mechanisms of Cr(VI) and Cr(III) by biochar supported nanosized zero-valent iron:
759 Synergy of adsorption, reduction and transformation, Environ. Pollut. 265 (2020)
760 115018. https://doi.org/10.1016/j.envpol.2020.115018.

761 [28] K. Li, Y. Hanpei, W. Lina, C. Siqi, Z. Ruichen, W. Junming, L. Xiaona, Facile
762 integration of FeS and titanate nanotubes for efficient removal of total Cr from
763 aqueous solution: Synergy in simultaneous reduction of Cr(VI) and adsorption of
764 Cr(III), J. Hazard. Mater. 398 (2020).
765 https://doi.org/10.1016/j.jhazmat.2020.122834.

766 [29] X. Wang, J. Xu, J. Liu, J. Liu, F. Xia, C. Wang, R.A. Dahlgren, W. Liu, Mechanism of
767 Cr(VI) removal by magnetic greigite/biochar composites, Sci. Total Environ. 700
768 (2020) 134414. https://doi.org/10.1016/j.scitotenv.2019.134414.

769 [30] Y. Zhang, N. Liu, Y. Yang, J. Li, S. Wang, J. Lv, R. Tang, Novel carbothermal

synthesis of Fe, N co-doped oak wood biochar (Fe/N-OB) for fast and effective Cr(VI) removal, Colloids Surfaces A Physicochem. Eng. Asp. 600 (2020) 124926. https://doi.org/10.1016/j.colsurfa.2020.124926.

[31] Y. Zhang, S. Yang, T. Ren, Y. Zhang, Y. Jiang, Y. Xue, M. Wang, H. Chen, Y. Chen, Enhancing surface gully erosion of micron-sized zero-valent aluminum (mZVAl) for Cr(VI) removal: Performance and mechanism in the presence of carbonate buffer, J. Clean. Prod. 238 (2019) 117943. https://doi.org/10.1016/j.jclepro.2019.117943.

[32] X. Ruan, H. Liu, X. Ning, D. Zhao, X. Fan, Screening for the action mechanisms of Fe and Ni in the reduction of Cr(VI) by Fe/Ni nanoparticles, Sci. Total Environ. 715 (2020) 136822. https://doi.org/10.1016/j.scitotenv.2020.136822.

[33] W. Wang, P. Gao, C. Yang, Z. Zhao, S. Zhen, Y. Zhou, T. Zhang, Separable and reactivated magnetic mZVAl/nFe3O4 composite induced by ball milling for efficient adsorption-reduction- sequestration of aqueous Cr(VI), Sep. Purif. Technol. 288 (2022) 120689. https://doi.org/10.1016/j.seppur.2022.120689.

[34] X. Zeng, Y. Wang, X. He, C. Liu, X. Wang, X. Wang, Enhanced removal of Cr(VI) by reductive sorption with surface-modified Ti3C2Tx MXene nanocomposites, J. Environ. Chem. Eng. 9 (2021) 106203. https://doi.org/10.1016/j.jece.2021.106203.

[35] Y. Wang, N. Lin, Y. Gong, R. Wang, X. Zhang, Cu–Fe embedded cross-linked 3D hydrogel for enhanced reductive removal of Cr(VI): Characterization, performance, and mechanisms, Chemosphere. 280 (2021) 130663. https://doi.org/10.1016/j.chemosphere.2021.130663.

[36] W.M. Haynes, D.R. Lide, T.J. Bruno, CRC Handbook of Chemistry and Physics, 95th ed., CRC Press, Taylor & Francis Group, New York, NY, 2014.

[37] T. Asimakidou, D. Karfaridis, K. Kalaitzidou, K. Simeonidis, K. Chrissafis,

Optimization of tin oxyhydroxide-decorated biochar for improved hexavalent chromium uptake from drinking water, J. Environ. Chem. Eng. 10 (2022) 108051. https://doi.org/10.1016/j.jece.2022.108051.

[38] N. Guo, X. Lv, Q. Yang, X. Xu, H. Song, Effective removal of hexavalent chromium from aqueous solution by ZnCl2 modified biochar: Effects and response sequence of the functional groups, J. Mol. Liq. 334 (2021) 116149. https://doi.org/10.1016/j.molliq.2021.116149.

[39] X. Jian, S. Li, Y. Feng, X. Chen, R. Kuang, B. Li, Y. Sun, Influence of Synthesis Methods on the High-Efficiency Removal of Cr(VI) from Aqueous Solution by Fe-Modified Magnetic Biochars, ACS Omega. 5 (2020) 31234–31243. https://doi.org/10.1021/acsomega.0c04616.

[40] F. Chen, S. Guo, Y. Wang, L. Ma, B. Li, Z. Song, L. Huang, W. Zhang, Concurrent adsorption and reduction of chromium(VI) to chromium(III) using nitrogen-doped porous carbon adsorbent derived from loofah sponge, Front. Environ. Sci. Eng. 16 (2022) 1–11. https://doi.org/10.1007/s11783-021-1491-6.

[41] F. Liu, S. Hua, C. Wang, M. Qiu, L. Jin, B. Hu, Adsorption and reduction of Cr(VI) from aqueous solution using cost-effective caffeic acid functionalized corn starch, Chemosphere. 279 (2021) 130539. https://doi.org/10.1016/j.chemosphere.2021.130539.

[42] Q. Wang, J. Wen, X. Hu, L. Xing, C. Yan, Immobilization of Cr(VI) contaminated soil using green-tea impregnated attapulgite, J. Clean. Prod. 278 (2021) 123967. https://doi.org/10.1016/j.jclepro.2020.123967.

[43] A.P. Rawat, D.P. Singh, Synergistic action of adsorption and reductive properties of ash derived from distilled Mentha piperita plant waste in removal of Cr(VI) from

aqueous solution, Ecotoxicol. Environ. Saf. 176 (2019) 27–33. https://doi.org/10.1016/j.ecoenv.2019.03.067.

[44] M. Ibrahim, M. Labaki, J.-M. Giraudon, J.-F. Lamonier, Hydroxyapatite, a multifunctional material for air, water and soil pollution control: A review, J. Hazard. Mater. 383 (2020) 121139. https://doi.org/10.1016/j.jhazmat.2019.121139.

[45] M. Ferri, S. Campisi, L. Polito, J. Shen, A. Gervasini, Tuning the sorption ability of hydroxyapatite/carbon composites for the simultaneous remediation of wastewaters containing organic-inorganic pollutants, J. Hazard. Mater. 420 (2021) 126656. https://doi.org/10.1016/j.jhazmat.2021.126656.

[46] M. Ferri, S. Campisi, A. Gervasini, Nickel and cobalt adsorption on hydroxyapatite: a study for the de-metalation of electronic industrial wastewaters, Adsorption. 25 (2019) 649–660. https://doi.org/10.1007/s10450-019-00066-w.

[47] M. Ferri, S. Campisi, M. Scavini, C. Evangelisti, P. Carniti, A. Gervasini, In-depth study of the mechanism of heavy metal trapping on the surface of hydroxyapatite, Appl. Surf. Sci. 475 (2019) 397–409. https://doi.org/10.1016/j.apsusc.2018.12.264.

[48] S. Campisi, C. Castellano, A. Gervasini, Tailoring the structural and morphological properties of hydroxyapatite materials to enhance the capture efficiency towards copper(II) and lead(II) ions, New J. Chem. 42 (2018) 4520–4530. https://doi.org/10.1039/c8nj00468d.

[49] S. Campisi, C. Evangelisti, G. Postole, A. Gervasini, Combination of interfacial reduction of hexavalent chromium and trivalent chromium immobilization on tin-functionalized hydroxyapatite materials, Appl. Surf. Sci. 539 (2021) 148227. https://doi.org/10.1016/j.apsusc.2020.148227.

[50] E. Rodrigues, O. Almeida, H. Brasil, D. Moraes, M.A.L. dos Reis, Adsorption of

chromium (VI) on hydrotalcite-hydroxyapatite material doped with carbon nanotubes: Equilibrium, kinetic and thermodynamic study, Appl. Clay Sci. 172 (2019) 57–64. https://doi.org/10.1016/j.clay.2019.02.018.

[51] S. Hokkanen, A. Bhatnagar, E. Repo, S. Lou, M. Sillanpää, Calcium hydroxyapatite microfibrillated cellulose composite as a potential adsorbent for the removal of Cr(VI) from aqueous solution, Chem. Eng. J. 283 (2016) 445–452. https://doi.org/10.1016/j.cej.2015.07.035.

[52] S. Periyasamy, V. Gopalakannan, N. Viswanathan, Hydrothermal assisted magnetic nano-hydroxyapatite encapsulated alginate beads for efficient Cr(VI) uptake from water, J. Environ. Chem. Eng. 6 (2018) 1443–1454. https://doi.org/10.1016/j.jece.2018.01.007.

[53] V. Gopalakannan, S. Periyasamy, N. Viswanathan, Fabrication of magnetic particles reinforced nano-hydroxyapatite/gelatin composite for selective Cr(vi) removal from water, Environ. Sci. Water Res. Technol. 4 (2018) 783–794. https://doi.org/10.1039/c8ew00027a.

[54] R. Al-Wafi, M.K. Ahmed, S.F. Mansour, Tuning the synthetic conditions of graphene oxide/magnetite/ hydroxyapatite/cellulose acetate nanofibrous membranes for removing Cr(VI), Se(IV) and methylene blue from aqueous solutions, J. Water Process Eng. 38 (2020) 101543. https://doi.org/10.1016/j.jwpe.2020.101543.

[55] P. Karthikeyan, S.S.D. Elanchezhiyan, H.A.T. Banu, M. Hasmath Farzana, C.M. Park, Hydrothermal synthesis of hydroxyapatite-reduced graphene oxide (1D–2D) hybrids with enhanced selective adsorption properties for methyl orange and hexavalent chromium from aqueous solutions, Chemosphere. 276 (2021) 130200. https://doi.org/10.1016/j.chemosphere.2021.130200.

[56] M.G. Galloni, S. Campisi, S.G. Marchetti, A. Gervasini, Environmental reactions of air-quality protection on eco-friendly iron-based catalysts, Catalysts. 10 (2020) 1–19. https://doi.org/10.3390/catal10121415.

[57] S. Campisi, M.G. Galloni, S.G. Marchetti, A. Auroux, G. Postole, A. Gervasini, Functionalized Iron Hydroxyapatite as Eco-friendly Catalyst for NH3-SCR Reaction: Activity and Role of Iron Speciation on the Surface, ChemCatChem. 12 (2020) 1676–1690. https://doi.org/10.1002/cctc.201901813.

[58] R. Baird, L. Bridgewater, Standard Methods for the Examination of Water and Wastewater, 23rd ed., American Public Health Association, Washington, D.C., 2017.

[59] D.T. Nguyen, C. Zeng, S. Sinha, P. Westerhoff, Stannous Chloride Reductive Treatment and Kinetics Using Hexavalent Chromium in Water Supplies, Environ. Eng. Sci. 37 (2020) 649–657. https://doi.org/10.1089/ees.2020.0063.

[60] J. Wang, X. Guo, Adsorption kinetic models: Physical meanings, applications, and solving methods, J. Hazard. Mater. 390 (2020) 122156. https://doi.org/10.1016/j.jhazmat.2020.122156.

[61] Y. Xu, J. Chen, R. Chen, P. Yu, S. Guo, X. Wang, Adsorption and reduction of chromium(VI) from aqueous solution using polypyrrole/calcium rectorite composite adsorbent, Water Res. 160 (2019) 148–157. https://doi.org/10.1016/j.watres.2019.05.055.

[62] B.M. Weckhuysen, I.E. Wachs, R.A. Schoonheydt, Surface chemistry and spectroscopy of chromium in inorganic oxides, Chem. Rev. 96 (1996) 3327–3349. https://doi.org/10.1021/cr9400440.

[63] P. Manjunathan, V.S. Marakatti, P. Chandra, A.B. Kulal, S.B. Umbarkar, R. Ravishankar, G. V. Shanbhag, Mesoporous tin oxide: An efficient catalyst with

versatile applications in acid and oxidation catalysis, Catal. Today. 309 (2018) 61–76. https://doi.org/10.1016/j.cattod.2017.10.009.

[64] M. Boronat, P. Concepción, A. Corma, M. Renz, Peculiarities of Sn-Beta and potential industrial applications, Catal. Today. 121 (2007) 39–44. https://doi.org/10.1016/j.cattod.2006.11.010.

[65] H. Chang, X. Chen, J. Li, L. Ma, C. Wang, C. Liu, J.W. Schwank, J. Hao, Improvement of activity and SO2 tolerance of Sn-modified MnOx-CeO2 catalysts for NH3-SCR at low temperatures, Environ. Sci. Technol. 47 (2013) 5294–5301. https://doi.org/10.1021/es304732h.

[66] A.E. Palomares, J.G. Prato, F.E. Imbert, A. Corma, Catalysts based on tin and beta zeolite for the reduction of NOx under lean conditions in the presence of water, Appl. Catal. B Environ. 75 (2007) 88–94. https://doi.org/10.1016/j.apcatb.2007.03.013.

[67] A. Karami, V. Salehi, The influence of chromium substitution on an iron-titanium catalyst used in the selective catalytic reduction of NO, J. Catal. 292 (2012) 32–43. https://doi.org/10.1016/j.jcat.2012.04.007.

[68] M.A. Zamudio, N. Russo, D. Fino, Low temperature NH3 selective catalytic reduction of NO x over substituted MnCr2O4 spinel-oxide catalysts, Ind. Eng. Chem. Res. 50 (2011) 6668–6672. https://doi.org/10.1021/ie200227u.

[69] P.M. Sreekanth, D.A. Peña, P.G. Smirniotis, Titania supported bimetallic transition metal oxides for low-temperature SCR of NO with NH 3, Ind. Eng. Chem. Res. 45 (2006) 6444–6449. https://doi.org/10.1021/ie060485l.

[70] M. Qiu, S. Zhan, D. Zhu, H. Yu, Q. Shi, NH3-SCR performance improvement of mesoporous Sn modified Cr-MnOx catalysts at low temperatures, Catal. Today. 258 (2015) 103–111. https://doi.org/10.1016/j.cattod.2015.03.049.

[71] M. Ferri, L. Delafontaine, S. Guo, T. Asset, P. Cristiani, S. Campisi, A. Gervasini, P. Atanassov, Steering Cu-Based CO 2 RR Electrocatalysts' Selectivity: Effect of Hydroxyapatite Acid/Base Moieties in Promoting Formate Production , ACS Energy Lett. (2022) 2304–2310. https://doi.org/10.1021/acsenergylett.2c01144.

[72] S. Campisi, M.G. Galloni, F. Bossola, A. Gervasini, Comparative performance of copper and iron functionalized hydroxyapatite catalysts in NH3-SCR, Catal. Commun. 123 (2019) 79–85. https://doi.org/10.1016/j.catcom.2019.02.008.

[73] S. Campisi, S. Palliggiano, A. Gervasini, C. Evangelisti, Finely Iron-Dispersed Particles on β Zeolite from Solvated Iron Atoms: Promising Catalysts for NH3-SCO, J. Phys. Chem. C. 123 (2019) 11723–11733. https://doi.org/10.1021/acs.jpcc.9b01474.

[74] G. Comino, A. Gervasini, V. Ragaini, Z.R. Ismagilov, Methane combustion over copper chromite catalysts, Catal. Letters. 48 (1997) 39–46. https://doi.org/10.1023/A:1019070819421.

CRediT author statement

Sebastiano Campisi: Conceptualization, Methodology, Validation, Writing- Original draft preparation, reviewing and editing, Supervision. **Mirko Leone**: Investigation, Data curation. **Maddalena Papacchini:** Funding Acquisition. **Claudio Evangelisti***:* Investigation, Data curation. **Laura Polito***:* Investigation, Data curation. **Georgeta Postole***:* Investigation, Data curation. **Antonella Gervasini**: Conceptualization, Methodology, Validation, Writing- Reviewing and Editing, Supervision.

Declaration of interests

☒The authors declare that they have no known competing financial interests or personal relationships that could have appeared to influence the work reported in this paper.

☐The authors declare the following financial interests/personal relationships which may be considered as potential competing interests: